


RESEARCH ARTICLE

Fixed-time control for free-floating space manipulators with prescribed constraints and input saturation

Y.X. Yan¹ , H.T. Cui^{1,2} and P. Han²

¹Deep Space Exploration Research Center, Harbin Institute of Technology, Harbin, China and ²School of Civil Engineering, Harbin Institute of Technology, Harbin, China

Corresponding author: Y.X. Yan; Email: yanyxhit@126.com

Received: 9 May 2023; Revised: 24 September 2023; Accepted: 25 September 2023

Keywords: space manipulator; trajectory tracking; PPC; sliding mode control

Abstract

This paper investigates the issue of tracking control for a free-floating space manipulator with prescribed performance constraints, considering the inertia uncertainties, internal disturbances and input saturation. An inherently continuous adaptive controller is proposed by incorporating non-singular fixed-time sliding mode control, prescribed performance control (PPC), and auxiliary compensation. First, a modified non-singular fast fixed-time terminal sliding surface is constructed, which has a shorter convergence time than the conventional fixed-time sliding surface. Unlike the existing complicated PPCs, a simple structure controller is developed to satisfy prescribed performance constraints through a unique tangent-type PPC technique. The input saturation is then compensated adaptively by an auxiliary mechanism. The Lyapunov theory thoroughly validates the stability and fixed-time convergence of the closed-loop tracking system. With the suggested control scheme, the system states can converge quickly to a small neighbourhood around the origin within a preassigned time, while the position tracking error can be confined within a prescribed performance bounds even in the presence of input saturation. Compared to the existing tracking methods, the suggested control approach has the advantages of faster transient convergence, higher steady-state tracking precision, and stronger robustness. Simulation comparisons demonstrate the effectiveness and superiority of the proposed controller.

Nomenclature

$\mathbf{H}(\mathbf{q})$	positive definite symmetric inertia matrix
$\mathbf{C}(\mathbf{q}, \dot{\mathbf{q}})$	coriolis and centrifugal matrix
$\mathbf{q}, \dot{\mathbf{q}}, \ddot{\mathbf{q}}$	generalized position, velocity and acceleration vector
\mathbf{u}	the input control torque
\mathbf{u}_c	the desired torque command
\mathbf{d}	represent the bounded disturbances
\mathbf{e}_1	trajectory tracking error
\mathbf{e}_2	velocity tracking error
\mathbf{s}	sliding surface
\mathbf{f}_{dis}	unknown lumped uncertain term
\mathbf{q}_d	the desired motion trajectory
$\dot{\mathbf{q}}_d$	the desired motion velocity trajectory
$b_c, b_n, b_m, a_n, b_1, b_2, b_3, b_4$	positive constants
c_1, c_2, c_3	unknown constants
m_1, n_1	positive constants
p, q	positive odd integers
ρ	a positive continuous function
$\mathbf{K}_1, \mathbf{K}_2, \boldsymbol{\eta}, \boldsymbol{\zeta}$	positive definite matrices

ε_N arbitrary small positive constant
 Ω auxiliary variable

1.0 Introduction

With the increasing number of orbital debris and failed satellites, space manipulator technologies aimed at active debris removal and on-orbit maintenance have received widespread attention [1, 2]. To conserve fuel consumption, the space manipulator applied to on-orbit missions normally has a free-floating spacecraft base. As the spacecraft's thrusters are turned off, there is a strong coupling between the manipulator and the spacecraft's base. That is, any movement of the manipulator interferes unfavourably with the translation and rotation of the spacecraft base. Such a characteristic makes the tracking control of the space manipulator more challenging than that of the terrestrial manipulator. Besides, the space manipulator is inevitably subject to parametric uncertainties and environmental perturbations, degrading system control performance and even destabilising the whole system. To address these issues, many control methodologies have been introduced into the trajectory tracking of space manipulators, for instance, adaptive control [3, 4], robust control [5, 6], sliding mode control (SMC) [7, 8] and neural network control [9, 10].

The majority of the aforementioned approaches, however, only guarantee the asymptotic stability of tracking errors with infinite convergence time. In pursuit of faster response and higher tracking precision, finite-time control (FTC) schemes have been frequently implemented in the trajectory tracking of manipulators. A terminal sliding mode control (TSMC) was presented for a space rigid manipulator sensitive to external disturbance to accomplish the finite-time state convergence [11]. Feng et al. [12] constructed a global non-singular terminal sliding mode control (NTSMC) to overcome the singularity problem existing in the traditional TSMCs. Based on adaptive NTSMC, a finite-time trajectory controller was also investigated for a space manipulator considering actuator saturation simultaneously [13]. In Ref. [14], a continuous singularity-free fast terminal sliding mode control (FTSMC) was put forward to speed up the convergence rate, especially when the state was far from the equilibrium point. Shao et al. [15] proposed NTSMC for the finite-time trajectory tracking of free-floating space manipulator with unknown disturbances, which enhanced the transient performance of the system and reduced the perturbations to the spacecraft base. A continuous non-singular integral sliding mode control (NISMC) was also presented for the finite-time fault-tolerant control of space manipulators to deal with different undesirable actuator faults [16]. Nevertheless, the settling time required in these FTC schemes is sensitive to the system's initial conditions, which makes it difficult to obtain a prior accurate estimation of the convergence time. Considering this fact, the concept of fixed-time stabilisation was firstly proposed by Polyakov [17]. The significant property of this method is that the upper bound of the settling time is only determined by predefined control parameters regardless of initial states. Due to such an excellent feature, fixed-time control strategies have received a lot of popularity in the field of nonlinear system control [18–21]. In particular, an observer-based fixed-time control scheme was developed for the task-space trajectory tracking of a space manipulator with external disturbances [22]. In Ref. [23], a non-singular TSMC was proposed to guarantee the fixed-time tracking stabilisation of a robot manipulator system despite parameter uncertainties and external disturbances. By combining an adaptive mechanism, a non-singular fixed-time SMC scheme was then developed for trajectory tracking of an uncertain manipulator under actuator saturation [24].

Whilst the transient performance, which is crucial to executing the task of trajectory tracking, has been overlooked in the aforementioned efforts. Due to the absence of prior information about the distant environment or objects, the system states should be restricted to specific predefined ranges to avoid accidental collisions between the space manipulator and objects. Therefore, it is necessary to take the impact of output state constraints on system performance into consideration. An adaptive fuzzy neural network (NN) control was derived for a constrained robot [25], where a barrier Lyapunov function was employed for performance improvement. The barrier Lyapunov function technique solely focuses

on the qualitative treatment of boundary constraints rather than the quantitative evaluation of dynamic performance constraints. As is well known, the PPC [26] is an appropriate choice for quantitatively characterising dynamic and steady-state performances in advance. The tracking error is confined in this approach inside the envelope described by the specified performance function, so as to achieve the desired transient and steady-state performances. Its primary idea is the use of error transformation to transform the original constrained dynamics into an equivalent unconstrained one. Thereby, the performance metrics, such as convergence time, steady-state error and overshoot, are assured to satisfy the predefined requirements on the premise of preserving the unconstrained system's stability. The concept of prescribed performance was first applied in the funnel control (FC) proposed in Ref. [27]. Compared with PPC, FC is usually limited to nonlinear systems with a relatively low-degree. Therefore, in recent years, PPC has been widely utilised in the control of robotic systems [28, 29], space vehicle systems [30, 31] and multi-agent systems [32], for the sake of ensuring the system's desired transient performance. And a new finite-time PPC (FPPC) is exploited in Ref. [33], which enables given-time convergence of tracking errors with small overshoot. Moreover, several studies have been conducted on the issue of tracking control for space manipulators considering prescribed performance constraints [34–36]. Although there are promising advances in the tracking control of space manipulators with specified performance, the existing methods have the following shortcomings:

- (1) There is a sluggish transient response, and large convergence time is necessary when system state is far from the equilibrium point.
- (2) The structure of PPC-based constraint controllers [37–39] is usually extremely sophisticated due to the full use of transformed error.
- (3) When considering input saturation, they have difficulty guaranteeing performance constraints and fixed-time tracking convergence.

Inspired by the above observations, a novel adaptive fixed-time control scheme with prescribed performance constraints is developed for trajectory tracking of the free-floating space manipulator subject to input saturation. Parameter uncertainties and unknown disturbances are also considered. More specifically, the main contributions of this paper are concisely summarised as follows:

- (1) A non-singular fast fixed-time terminal sliding surface is constructed to obtain a faster convergence rate than the existing fixed-time terminal sliding surfaces in Refs [40, 41].
- (2) To avoid the complexities associated with stabilising transformed error in conventional PPCs, a unique tan-type PPC technique is directly introduced in the control design. The structural simplicity of the designed controller allows for greater flexibility in practical applications.
- (3) The effect of actuator saturation is mitigated by an input saturation compensator. The resulting controller ensures that the fixed-time prescribed performance of the space manipulator is fulfilled, considering parameter uncertainties, unknown disturbances, and input saturation simultaneously.

The rest of this work is organised as follows. Section 2 represents the problem description and some required definitions. In Section 3, the processes of control design and stability analysis are given in detail. Section 4 discusses the simulation results, and draws conclusions in Section 5.

2.0 Problem description and preliminaries

2.1 Notations and lemmas

For an n -dimensional vector $x = [x_1, x_2, \dots, x_n]^T$ with the i th element x_i ($i = 1, 2, \dots, n$). The symbols $\|\cdot\|$ and $\|\cdot\|_1$ represent the Euclidean norm and 1-norm, respectively. For a constant $\gamma > 0$, define $\text{sig}^\gamma(x) = [|x_1|^\gamma \text{sign}(x_1), |x_2|^\gamma \text{sign}(x_2), \dots, |x_n|^\gamma \text{sign}(x_n)]^T$ and the vector $\text{sgn}(x) =$

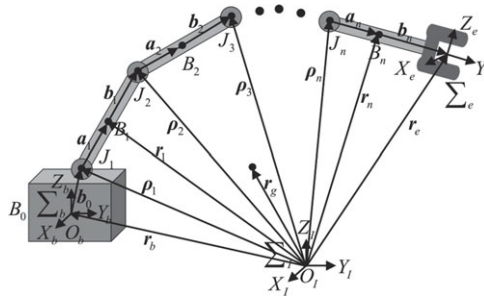


Figure 1. Space manipulator system model.

$[\text{sign}(x_1), \text{sign}(x_2), \dots, \text{sign}(x_n)]^T$, where $\text{sign}(\cdot)$ denotes the sign function. $I_n \in \mathbb{R}^{n \times n}$ is n-dimensional identity matrix.

Lemma 1. [42] Let $A_i \geq 0 (i = 1, 2, \dots, n)$, for $0 < p_1 \leq 1$ and $p_2 > 1$, the following inequalities hold

$$\sum_{i=1}^n A_i^{p_1} \geq \left(\sum_{i=1}^n A_i \right)^{p_1}, \quad \sum_{i=1}^n A_i^{p_2} \geq n^{1-p_2} \left(\sum_{i=1}^n A_i \right)^{p_2} \tag{1}$$

Definition 1 (Fixed-time stable). [17] Consider the nonlinear system

$$\dot{z}(t) = g(z(t)), z(0) = z_0, g(0) = 0, z \in \mathbb{R}^n \tag{2}$$

The origin of the system (2) is said to be fixed-time stable if it is finite-time stable and the convergence time $T(z_0)$ is bounded for any initial states, that is, $\exists T_{max} > 0$ such that $T(z_0) \leq T_{max}, \forall z_0 \in \mathbb{R}^n$.

Lemma 2 (Globally fixed-time stabilisation). [18] Suppose there exist one Lyapunov function $V(z)$, such that $\dot{V}(z) \leq -\alpha_0 V^{\eta_0}(z) - \beta_0 V^{\Gamma_0}(z)$ holds with $\alpha_0, \beta_0 > 0, \eta_0 > 1$, and $\Gamma_0 \in (0, 1)$. Then, the equilibrium of system (2) is globally fixed-time stable, and the settling time $T(z_0)$ is bounded by $T(z_0) \leq \frac{1}{\alpha_0(\eta_0-1)} + \frac{1}{\beta_0(1-\Gamma_0)}, \forall z_0 \in \mathbb{R}^n$.

Lemma 3 (Practical fixed-time stabilisation). [43] Suppose there is a Lyapunov function $V(z)$, and real number $0 < \vartheta_0 < \infty, \alpha_0, \beta_0 > 0, \eta_0 > 1$, and $\Gamma_0 \in (0, 1)$, such that $\dot{V}(z) \leq -\alpha_0 V^{\eta_0}(z) - \beta_0 V^{\Gamma_0}(z) + \vartheta_0$ holds. Then, the system (2) is practical fixed-time stable and the system can be stabilised within the residual set containing the equilibrium point in a fixed time. For $\theta_1, \theta_2 \in (0, 1]$, the residual set is presented as $D_s = \left\{ \lim_{t \rightarrow T} z \mid V(z) \leq \min \left\{ \alpha_0^{-1/\eta_0} \left(\frac{\vartheta_0}{1-\theta_1} \right)^{1/\eta_0}, \beta_0^{-1/\Gamma_0} \left(\frac{\vartheta_0}{1-\theta_2} \right)^{1/\Gamma_0} \right\} \right\}$ and the upper bound of convergence time is given by $T(z_0) \leq \frac{1}{\alpha_0(\eta_0-1)} + \frac{1}{\beta_0(1-\Gamma_0)}, \forall z_0 \in \mathbb{R}^n$.

2.2 Space manipulator model

In the presence of disturbances, the dynamic equation of the free-floating space manipulator shown in Fig. 1 can be expressed as [15]:

$$\mathbf{H}(\mathbf{q}) \ddot{\mathbf{q}} + \mathbf{C}(\mathbf{q}, \dot{\mathbf{q}}) \dot{\mathbf{q}} = \mathbf{u} + \mathbf{d}(t) \tag{3}$$

where, $\mathbf{H}(\mathbf{q}) \in \mathbb{R}^{n \times n}$ is the positive definite symmetric inertia matrix. $\mathbf{C}(\mathbf{q}, \dot{\mathbf{q}}) \in \mathbb{R}^{n \times n}$ denotes the Coriolis and centrifugal matrix. $\mathbf{q}, \dot{\mathbf{q}}, \ddot{\mathbf{q}} \in \mathbb{R}^n$ represent the generalised position, velocity and acceleration vector, respectively. $\mathbf{u} \in \mathbb{R}^n$ is the input control torque, and $\mathbf{d}(t) \in \mathbb{R}^n$ represents the bounded disturbances caused by internal factors, satisfying $\|\mathbf{d}\| < d_0$ with d_0 is an unknown positive constant.

Noticed that matrices $\mathbf{H}(\mathbf{q})$ and $\mathbf{C}(\mathbf{q}, \dot{\mathbf{q}})$ always contain uncertainties, which can be further described as:

$$\mathbf{H}(\mathbf{q}) = \mathbf{H}_0(\mathbf{q}) + \Delta\mathbf{H}(\mathbf{q}), \tag{4}$$

$$\mathbf{C}(\mathbf{q}, \dot{\mathbf{q}}) = \mathbf{C}_0(\mathbf{q}, \dot{\mathbf{q}}) + \Delta\mathbf{C}(\mathbf{q}, \dot{\mathbf{q}}) \tag{5}$$

where, $\mathbf{H}_0(\mathbf{q})$ and $\mathbf{C}_0(\mathbf{q}, \dot{\mathbf{q}})$ represent the nominal parts, $\Delta\mathbf{H}(\mathbf{q})$ and $\Delta\mathbf{C}(\mathbf{q}, \dot{\mathbf{q}})$ denote the uncertainty parts.

Assumption 1. [44] *The norm of inertia matrix $\mathbf{H}(\mathbf{q})$ is upper bounded by a nonnegative finite constant a_n , i.e. $\|\mathbf{H}(\mathbf{q})\| < a_n$. Besides, there always exist constants $b_c, b, b_n \in \mathbb{R}^+$, such that $\|\mathbf{C}(\mathbf{q}, \dot{\mathbf{q}})\dot{\mathbf{q}}\| < b_c + b_n \|\mathbf{q}\| + b_m \|\dot{\mathbf{q}}\|^2$ holds.*

Define $\mathbf{x}_1 = \mathbf{q}$ and $\mathbf{x}_2 = \dot{\mathbf{q}}$, the modified dynamic model can be reformulated as:

$$\begin{cases} \dot{\mathbf{x}}_1 = \mathbf{x}_2 \\ \dot{\mathbf{x}}_2 = \mathbf{F}(\mathbf{x}_1, \mathbf{x}_2) + \mathbf{B}(\mathbf{x}_1) \mathbf{u} + \mathbf{f}_{dis} \end{cases} \tag{6}$$

where $\mathbf{F}(\mathbf{x}_1, \mathbf{x}_2) = -\mathbf{H}_0^{-1}(\mathbf{x}_1) \mathbf{C}_0(\mathbf{x}_1, \mathbf{x}_2)\mathbf{x}_2$, $\mathbf{B}(\mathbf{x}_1) = \mathbf{H}_0^{-1}(\mathbf{x}_1)$, and \mathbf{f}_{dis} stands for an unknown lumped uncertain term including unknown disturbances and model uncertainties, which is expressed as

$$\mathbf{f}_{dis} = \mathbf{H}_0^{-1}(\mathbf{x}_1) (\mathbf{d}(t) - \Delta\mathbf{C}(\mathbf{x}_1, \mathbf{x}_2)\mathbf{x}_2 - \Delta\mathbf{H}(\mathbf{x}_1) \dot{\mathbf{x}}_2) \tag{7}$$

Assumption 2. [45] *Since both the unknown disturbances and the inertial uncertainties are bounded, it is reasonable to assume the lumped uncertainty \mathbf{f}_{dis} is bounded, satisfying $\|\mathbf{f}_{dis}\| \leq c_1 + c_2 \|\mathbf{x}_1\| + c_3 \|\mathbf{x}_2\|^2 = \mathbf{c}_z^T \theta$ where $\theta = [1, \|\mathbf{x}_1\|, \|\mathbf{x}_2\|^2]^T$ and $\mathbf{c}_z = [c_1, c_2, c_3]^T$ with unknown constants $c_1, c_2, c_3 > 0$.*

Owing to the physical limitations of the actuators, the control torque \mathbf{u} is restricted by the saturation value, which can be expressed as

$$\mathbf{u} = \text{sat}(\mathbf{u}_c) \tag{8}$$

where $\mathbf{u}_c = [u_{c1}, u_{c2}, \dots, u_{cn}]^T \in \mathbb{R}^n$ is the desired torque command, and the saturation function $\text{sat}(\cdot)$ represents saturation nonlinear characteristics of the actuator with $\text{sat}(u_{ci}) = \text{sign}(u_{ci}) \cdot \min\{|u_{ci}|, u_{cimax}\}$, where u_{cimax} is the allowable maximum input torque of the i th actuator. Obviously, the saturation nonlinear term $\text{sat}(\mathbf{u}_c)$ can be abbreviated as the following form:

$$\text{sat}(\mathbf{u}_c) = \mathbf{u}_c + \delta_c \tag{9}$$

where, $\delta_c = [\delta_{c1}, \delta_{c2}, \dots, \delta_{cn}]^T \in \mathbb{R}^n$ denotes the saturation degree of the actuators, satisfying $|\delta_{ci}| \leq l_\delta$ with $l_\delta > 0$, and δ_{ci} is defined as

$$\delta_{ci} = \begin{cases} 0, & |u_{ci}| \leq u_{cimax} \\ \text{sign}(u_{ci}) \cdot u_{cimax} - u_{ci}, & |u_{ci}| > u_{cimax} \end{cases} \tag{10}$$

2.3 Problem formulation

To address the trajectory tracking issue of the space manipulator, the trajectory tracking error \mathbf{e}_1 and velocity tracking error \mathbf{e}_2 are defined as

$$\mathbf{e}_1 = \mathbf{x}_1 - \mathbf{q}_d, \mathbf{e}_2 = \mathbf{x}_2 - \dot{\mathbf{q}}_d \tag{11}$$

where $\mathbf{q}_d \in \mathbb{R}^n$ and $\dot{\mathbf{q}}_d \in \mathbb{R}^n$ are the desired motion and corresponding time derivative, respectively.

Considering the input saturation, the tracking error equation of the space manipulator can be derived:

$$\begin{cases} \dot{\mathbf{e}}_1 = \mathbf{e}_2 \\ \dot{\mathbf{e}}_2 = \mathbf{F}(\mathbf{x}_1, \mathbf{x}_2) + \mathbf{B}(\mathbf{x}_1) \mathbf{u}_c + \mathbf{B}(\mathbf{x}_1) \delta_c + \mathbf{f}_{dis} - \ddot{\mathbf{q}}_d \end{cases} \tag{12}$$

The main control objective of this paper is to design a tracking control command \mathbf{u}_c , such that

1. All signals in the closed-loop system are bounded.
2. Trajectory tracking is fulfilled within a specific time regardless of initial states.
3. The position tracking error is always confined within the prescribed performance bounds despite the presence of unknown disturbances, parameter uncertainties and input saturation.

3.0 Controller design and stability analysis

In this section, a continuous adaptive fixed-time sliding mode control method is designed for the free-floating space manipulator system. A novel constraint method based on the prescribed performance function is presented to handle the tracking error constraint issue. Considering the effects of input saturation, an auxiliary compensator is constructed to attain fixed-time stability.

3.1 Non-singular fast terminal slide mode surface

To improve the convergence property, the following non-singularity fast terminal sliding surface (NFTSS) is designed as

$$\mathbf{s} = \mathbf{e}_2 + N(\mathbf{e}_1) (\mathbf{K}_1 \text{sig}^{1+\sigma_1}(\mathbf{e}_1) + \mathbf{K}_2 \mathbf{s}_\rho(\mathbf{e}_1)) \tag{13}$$

where sliding surface $\mathbf{s} = [s_1, s_2, \dots, s_n]^T \in \mathbb{R}^n$. $N(\mathbf{e}_1) = 1 + 2s_m \arctan(s_n \|\mathbf{e}_1\|^{s_r}) / \pi$ with adjustable positive constants s_m, s_n and s_r . $\sigma_1 = \frac{m_1}{2n_1} (1 + \text{sgn}(\|\mathbf{e}_1\| - 1))$ with positive odd integers m_1, n_1 satisfying $m_1 > n_1$. $\mathbf{K}_1 = \text{diag}(K_{11}, K_{12}, \dots, K_{1n})$ and $\mathbf{K}_2 = \text{diag}(K_{21}, K_{22}, \dots, K_{2n})$ are positive definite matrices. $\mathbf{s}_\rho(\mathbf{e}_1) = [s_{\rho_1}, s_{\rho_2}, \dots, s_{\rho_n}]^T \in \mathbb{R}^n$ with s_{ρ_i} is defined as

$$s_{\rho_i} = \begin{cases} \text{sig}^{p/q}(e_{1i}), & \bar{s}_i = 0 \cup \bar{s}_i \neq 0, |e_{1i}| \geq \epsilon_0 \\ l_1 e_{1i} + l_2 e_{1i}^2 \text{sgn}(e_{1i}), & \bar{s}_i \neq 0, |e_{1i}| < \epsilon_0 \end{cases} \tag{14}$$

where $\bar{s}_i = e_{2i} + N(\mathbf{e}_1) (\mathbf{K}_{1i} \text{sig}^{1+\sigma_1}(e_{1i}) + \mathbf{K}_{2i} \text{sig}^{p/q}(e_{1i}))$. p, q are positive odd integers with $p < q$, and ϵ_0 is a small positive constant. To assure the sliding surface and its time derivative smooth and continuous, l_1 and l_2 are selected as

$$\begin{cases} l_1 = \left(2 - \frac{p}{q}\right) \epsilon_0^{p/q-1} \\ l_2 = \left(\frac{p}{q} - 1\right) \epsilon_0^{p/q-2} \end{cases} \tag{15}$$

Lemma 4. Consider the space manipulator system (12). Once the NFTSS (13) satisfies $s = 0$, then the system states e_1 and e_2 convergence to zero along the sliding surface in a fixed time for an arbitrary initial condition. The upper bound of settling time is given by

$$T_s \leq \max_{1 \leq i \leq n} \left\{ \frac{q}{K_{1i}(q-p)} \ln \left(1 + \frac{K_{1i}}{K_{2i}} \right) + \frac{n_1}{K_{1i} m_1} \right\} \tag{16}$$

Proof. Once the MFTSS is reached, i.e., $s = 0$, a series of the following differential equations can be obtained

$$e_{2i} + N(\mathbf{e}_1) (\mathbf{K}_{1i} \text{sig}^{1+\sigma_1}(e_{1i}) + \mathbf{K}_{2i} \text{sig}^{p/q}(e_{1i})) = 0, \quad i = 1, 2, \dots, n \tag{17}$$

Define a new variable as $Q = |e_{1i}|^{\frac{q-p}{q}}$, and the corresponding time-derivative is given by

$$\begin{aligned} \dot{Q} &= \frac{q-p}{q} \operatorname{sig}^{-\frac{p}{q}}(e_{1i}) e_{2i} \\ &= -\frac{(q-p)N(\mathbf{e}_1)}{q} \operatorname{sig}^{-\frac{p}{q}}(e_{1i}) (K_{1i} \operatorname{sig}^{1+\sigma_1}(e_{1i}) + K_{2i} \operatorname{sig}^{p/q}(e_{1i})) \\ &= -\frac{q-p}{q} N(\mathbf{e}_1) \left(K_{1i} |e_{1i}|^{\sigma_1 + \frac{q-p}{q}} + K_{2i} \right) \\ &= -\frac{q-p}{q} N(\mathbf{e}_1) \left(K_{1i} Q^{1 + \frac{\sigma_1 q}{q-p}} + K_{2i} \right) \end{aligned} \tag{18}$$

According to $N(\mathbf{e}_1) \geq 1$, the settling time T_{si} from $s_i = 0$ to $e_{1i} = 0$ along the sliding surface is determined by

$$\begin{aligned} T_{si} &= \frac{q}{(q-p)} \int_0^{Q(0)} \frac{1}{N(\mathbf{e}_1) \left(K_{1i} Q^{1 + \frac{\sigma_1 q}{q-p}} + K_{2i} \right)} dQ \\ &= \frac{q}{(q-p)} \int_0^1 \frac{1}{N(\mathbf{e}_1) \left(K_{1i} Q^{1 + \frac{\sigma_1 q}{q-p}} + K_{2i} \right)} dQ \\ &\quad + \frac{q}{(q-p)} \int_1^{Q(0)} \frac{1}{N(\mathbf{e}_1) \left(K_{1i} Q^{1 + \frac{\sigma_1 q}{q-p}} + K_{2i} \right)} dQ \\ &= \frac{q}{(q-p)} \int_0^1 \frac{1}{N(\mathbf{e}_1) (K_{1i} Q + K_{2i})} dQ \\ &\quad + \frac{q}{(q-p)} \int_1^{Q(0)} \frac{1}{N(\mathbf{e}_1) (K_{1i} Q^\psi + K_{2i})} dQ \\ &\leq \frac{q}{q-p} \left[\frac{1}{K_{1i}} \ln \left(1 + \frac{K_{1i}}{K_{2i}} \right) + \frac{1 - Q(0)^{1-\psi}}{K_{1i}(\psi - 1)} \right] \end{aligned} \tag{19}$$

where $\psi = 1 + \frac{m_1/n_1}{1-p/q}$. Due to $\psi > 1$ and $Q(0) > 1$, T_{si} is further bounded by

$$T_{si} \leq \frac{q}{K_{1i}(q-p)} \ln \left(1 + \frac{K_{1i}}{K_{2i}} \right) + \frac{n_1}{K_{1i}m_1} \tag{20}$$

Based on Equation (20), the upper bound of the convergence time T_s can be calculated by

$$T_s = \max_{1 \leq i \leq n} \{T_{si}\} \leq \max_{1 \leq i \leq n} \left\{ \frac{q}{K_{1i}(q-p)} \ln \left(1 + \frac{K_{1i}}{K_{2i}} \right) + \frac{n_1}{K_{1i}m_1} \right\} \tag{21}$$

From Equation (21), the upper bound of convergence time is independent of the system state values. It means that the tracking error \mathbf{e}_1 and its derivative \mathbf{e}_2 can converge to the origin within a refined time along the sliding surface. The proof is completed.

Remark 1. It should be pointed out that the strictly positive function $N(e_1)$ in NFTSS (13) is used to tune the convergence rate, which varies from $1 + s_m$ to 1. As the states are far from the origin, $N(e_1)$ approaches $1 + s_m$ that is greater than 1. Once the states are close to the origin, $N(e_1)$ tends to 1. The convergence rate is thus improved by introducing $N(e_1)$. Moreover, a new variable power term σ_1 is also included in the NFTSS, which can be adjusted according to the system states. When the states are in the vicinity of the origin, the NFTSS employs a linear term e_1 instead of nonlinear term $\operatorname{sig}^{\frac{m_1}{n_1}}(e_1)$, which results in a significant increase in the convergence rate. Therefore, the proposed NFTSS exhibits a superior convergence performance whether far from or within a small allowable range of the origin.

Remark 2. Huang et al. [40] presented a fixed-time sliding surface $s = e_2 + K_1 \text{sig}^{m_1/n_1}(e_1) + K_2 s_\rho(e_1)$ with $\bar{s}_i = e_{2i} + K_{1i} \text{sig}^{m_1/n_1}(e_{1i}) + K_{2i} \text{sig}^{p/q}(e_{1i})$, and derived the upper bound of convergence time $T_1 = \max_{1 \leq i \leq n} \left\{ \frac{q}{K_{2i}(q-p)} + \frac{n_1}{K_{1i}(m_1-n_1)} \right\}$. Another fast fixed-time sliding surface $s = e_2 + K_1 e_1^{\frac{1}{2} + \frac{m_1}{2n_1} + (\frac{m_1}{2n_1} - \frac{1}{2}) \text{sgn}(|e_1|^{-1})} + K_2 e_1^{\frac{q}{2}}$ is investigated in Ref. [41] and the settling time upper-bound was given by $T_2 = \max_{1 \leq i \leq n} \left\{ \frac{q}{K_{1i}(q-p)} \ln \left(1 + \frac{K_{1i}}{K_{2i}} \right) + \frac{n_1}{K_{1i}(m_1-n_1)} \right\}$. Since the relation $\ln(1 + K_{1i}/K_{2i}) < K_{1i}/K_{2i}$ holds, one has $T_s < T_2 < T_1$, which implies that under the same design parameters, the proposed NFTSS obtains the fastest convergence rate.

3.2 Prescribed performance function

Appropriate constraints on the system states are necessary to obtain the desired dynamic performance. With this in mind, the PPC is investigated to confine the position tracking error within a predefined permissible range here. First, describe such a constraint via a prescribed performance function, defined as follows.

Definition 2. [26] if a positive continuous function $\rho(t)$ satisfies 1) $\rho(t) > 0$ and $\dot{\rho}(t) \leq 0$ 2) $\lim_{t \rightarrow \infty} \rho(t) = \rho_\infty > 0$, then $\rho(t)$ is called a performance function.

Generally, a prescribed performance function is designed as

$$\rho(t) = (\rho_0 - \rho_\infty) e^{-l_0 t} + \rho_\infty \tag{22}$$

where $\rho_0 > \rho_\infty > 0$ and $l_0 > 0$ are design parameters and should be set appropriately to obtain the desired time-domain characteristics, such as steady-state offset, overshoot and rising time. As stated in Ref. [46], the prescribed performance is attained provided that the state is limited to the area bounded by the decaying function of time. According to the concept, achieving the prescribed error constraints is equivalent to satisfy the following relationship:

$$-\rho_i(t) < e_{1i}(t) < \rho_i(t) \tag{23}$$

where ρ_i denotes the prescribed performance function of s_i .

Based on the condition (23), one concludes that as long as $|e_{1i}(0)| < \rho_i(0)$ is satisfied, the tracking error is always never exceed the predefined boundary.

Remark 3. Define transformed constraint error z_i as $z_i = e_{1i}/\rho_i$. Obviously, when the constraint (23) is satisfied, z_i becomes $z_i \in (-1, 1)$. That is, when $|e_{1i}(t)|$ tends to the boundary $\rho_i(t)$, z_i approaches 1.

3.3 Fixed-time tracking controller design

Take the time derivative of s in Equation (13) and using Equation (12), one obtains

$$\begin{aligned} \dot{s} &= \mathbf{F}(\mathbf{x}_1, \mathbf{x}_2) + \mathbf{B}(\mathbf{x}_1) \mathbf{u}_c + \mathbf{B}(\mathbf{x}_1) \delta_c + \mathbf{f}_{dis} - \ddot{\mathbf{q}}_d \\ &+ \dot{N}(\mathbf{e}_1) (\mathbf{K}_1 \text{sig}^{1+\sigma_1}(\mathbf{e}_1) + \mathbf{K}_2 \mathbf{s}_\rho(\mathbf{e}_1)) \\ &+ N(\mathbf{e}_1) ((1 + \sigma_1) \mathbf{K}_1 \text{diag}(|e_{1i}|^{\sigma_1}) \mathbf{e}_2 + \mathbf{K}_2 \dot{\mathbf{s}}_\rho(\mathbf{e}_1)) \end{aligned} \tag{24}$$

where the i th element of $\dot{\mathbf{s}}_\rho$ is given by

$$\dot{s}_i = \begin{cases} \frac{p}{q} |e_{1i}|^{p/q-1} e_{2i}, & \bar{s}_i = 0 \cup \bar{s}_i \neq 0, |e_{1i}| \geq \epsilon_0 \\ l_1 e_{2i} + 2l_2 |e_{1i}| e_{2i}, & \bar{s}_i \neq 0, |e_{1i}| < \epsilon_0 \end{cases} \tag{25}$$

Aiming to attain trajectory tracking with high precision, the following adaptive nonsingular fixed-time sliding mode control with prescribed performance constraints is developed

$$\mathbf{u}_c = \mathbf{u}_{eq} + \mathbf{u}_r + \mathbf{u}_s \tag{26}$$

where,

$$\begin{aligned} \mathbf{u}_{eq} = & -\mathbf{B}^{-1}(\mathbf{x}_1) (\mathbf{F}(\mathbf{x}_1, \mathbf{x}_2) - \ddot{\mathbf{q}}_d) \\ & - \mathbf{B}^{-1}(\mathbf{x}_1) ((1 + \sigma_1)\mathbf{K}_1 \text{diag}(|e_{1i}|^{\sigma_1})\mathbf{e}_2 + \mathbf{K}_2 \dot{\mathbf{s}}_\rho(\mathbf{e}_1)) \\ & - \mathbf{B}^{-1}(\mathbf{x}_1) \dot{N}(\mathbf{e}_1) (\mathbf{K}_1 \text{sig}^{1+\sigma_1}(\mathbf{e}_1) + \mathbf{K}_2 \mathbf{s}_\rho(\mathbf{e}_1)) \end{aligned} \tag{27}$$

$$\begin{aligned} \mathbf{u}_r = & -\mathbf{B}^{-1}(\mathbf{x}_1) G(\mathbf{s}) (\gamma_1 \text{sig}^{1+\sigma_2}(\mathbf{s}) + \gamma_2 \text{sig}^{\beta_1}(\mathbf{s}) + \gamma_3 \mathbf{s}) \\ & - \mathbf{B}^{-1}(\mathbf{x}_1) \Gamma_4 \text{diag} \left\{ z_i \tan \left(\frac{\pi z_i}{2} \right) \right\} \mathbf{s} - \mathbf{B}^{-1}(\mathbf{x}_1) \frac{\hat{\mathbf{c}}_m^T \Theta}{2\epsilon_N^2} \mathbf{s} \end{aligned} \tag{28}$$

$$\mathbf{u}_s = -\mathbf{B}^{-1}(\mathbf{x}_1) \gamma_5 \Omega - \frac{1}{2} \mathbf{B}^{-1}(\mathbf{x}_1) \mathbf{s} \tag{29}$$

$$G(s) = 1 + \chi - \chi e^{-v_1 \|s\|^k} \tag{30}$$

where $\sigma_2 = \frac{\alpha_1}{2} (1 + \text{sgn}(|s| - 1))$ with $\alpha_1 > 1$, and $\beta_1 \in (0,1)$. $\chi > 0$, $v_1 > 0$ and k is a positive integer, $\gamma_1, \gamma_2, \gamma_3, \gamma_5$ are positive design parameters, $\Gamma_4 = \text{diag}(\gamma_{41}, \gamma_{42}, \dots, \gamma_{4m})$ is a positive constant matrix, which is used as the tuning gain to force the tracking error to remain within the defined boundary. $\hat{\mathbf{c}}_m$ is the estimation of \mathbf{c}_m with $\mathbf{c}_m = [c_1^2, c_2^2, c_3^2]^T$, and $\Theta = [1, \|\mathbf{x}_1\|^2, \|\mathbf{x}_2\|^4]^T$. The adaptive update law is designed as

$$\dot{\hat{\mathbf{c}}}_m = \eta \left(\frac{\Theta \|\mathbf{s}\|^2}{2\epsilon_N^2} - \zeta \hat{\mathbf{c}}_m \right) \tag{31}$$

where $\eta = \text{diag}(\eta_1, \eta_2, \eta_3)$ and $\zeta = \text{diag}(\zeta_1, \zeta_2, \zeta_3)$ are two positive matrices, and ϵ_N is an arbitrary small positive constant.

To compensate for input saturation, the auxiliary variable Ω is given by

$$\dot{\Omega} = \begin{cases} 0, & \|\Omega\| \leq \Omega_0 \\ -b_1 \Omega^{1+\sigma_2} - b_2 \Omega^{\beta_1} - b_3 \Omega - \\ \frac{\|\mathbf{s}^T \mathbf{B}(\mathbf{x}_1) \delta_c\|_1 + 0.5 b_4 \delta_c^T \delta_c}{\|\Omega\|^2} \Omega + b_4 \delta c, & \|\Omega\| > \Omega_0 \end{cases} \tag{32}$$

where b_1, b_2, b_3, b_4 and Ω_0 are positive constants.

Remark 4. The auxiliary variable combined with fast terminal sliding mode control enables fixed-time convergence of tracking control. The parameter b_4 is intended to avoid the possible overcompensation of actuator saturation.

Remark 5. It is worth noting that when $|e_{1i}|$ approaches the constraint boundary ρ_i , then $z_i \rightarrow 1$, and the value of $\tan(\frac{\pi z_i}{2})$ tends to infinity. The control gain is thus increased to suppress the evolution of the tracking error. Figure 2 illustrates this constraint control scheme in graphical form. If the required control law is unreasonable or the evolution of tracking error violates the constraint boundaries, the values of ρ_0, ρ_∞, l_0 and Γ_4 must be adjusted according to practical application.

Lemma 5. Consider the space manipulator system (12) with the lumped uncertainty satisfying Assumption 2. If the sliding surface is defined as Equation (13) and the control laws are designed as Equations (26)–(30) with the adaptive update law Equation (31) and the auxiliary system Equation (32),

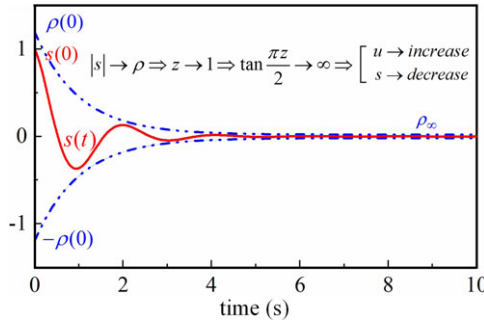


Figure 2. The description of the constraint control scheme.

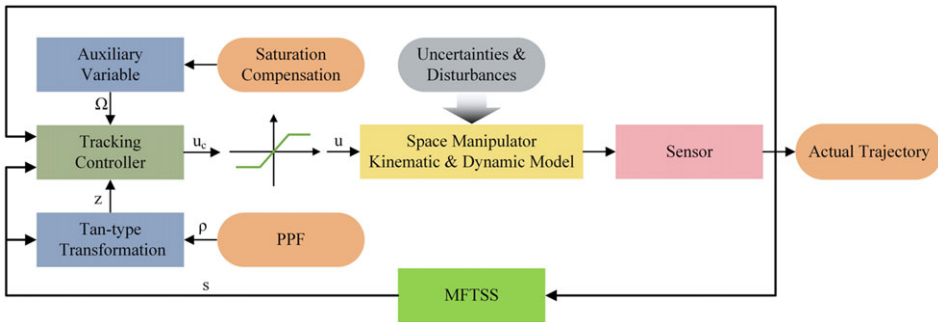


Figure 3. The structure of the proposed control scheme.

then the system trajectory enables to enforce into the vicinity of the sliding surface $s = 0$ from any initial states within a fixed time. Furthermore, system's tracking errors e_1 and e_2 converge to a small set containing the region.

For a deeper understanding of the overall structure of the suggested method, Fig. 3 shows the closed-loop tracking control system.

3.4 Stability analysis

To prove Lemma 5, the following will analyse and demonstrate in two steps.

Step 1. Fixed time convergence property of the sliding surface s is verified.

Substituting Equations (26)–(29) into Equation (24), one obtains

$$\begin{aligned} \dot{s} = & -G(s) (\gamma_1 \text{sig}^{1+\sigma_2}(s) + \gamma_2 \text{sig}^{\beta_1}(s) + \gamma_3 s) + \mathbf{B}(x_1) \delta_c \\ & - \Gamma_4 \text{diag} \left\{ z_i \tan \left(\frac{\pi z_i}{2} \right) \right\} s - \left(\frac{\tilde{\mathbf{c}}_m^T \Theta}{2\epsilon_N^2} + \frac{1}{2} \right) s - \gamma_5 \Omega + \mathbf{f}_{dis} \end{aligned} \tag{33}$$

To validate the stability of the closed-loop system, define the following Lyapunov function:

$$V_2 = \frac{1}{2} \mathbf{s}^T \mathbf{s} + \frac{1}{2} \tilde{\mathbf{c}}_m^T \boldsymbol{\eta}^{-1} \tilde{\mathbf{c}}_m + \frac{1}{2} \Omega^T \Omega \tag{34}$$

where $\tilde{\mathbf{c}}_m = \mathbf{c}_m - \hat{\mathbf{c}}_m$ denotes the estimate error of \mathbf{c}_m .

The derivative of V_2 with respect to time yields

$$\dot{V}_2 = \mathbf{s}^T \dot{s} - \tilde{\mathbf{c}}_m^T \boldsymbol{\eta}^{-1} \dot{\tilde{\mathbf{c}}}_m + \Omega^T \dot{\Omega} \tag{35}$$

Then, one can derive

$$\begin{aligned}
 \dot{V}_2 &= -\mathbf{s}^T \left\{ G(\mathbf{s}) (\gamma_1 \text{sig}^{1+\sigma_2}(\mathbf{s}) + \gamma_2 \text{sig}^{\beta_1}(\mathbf{s}) + \gamma_3 \mathbf{s}) - \mathbf{B}(\mathbf{x}_1) \delta_c \right. \\
 &\quad \left. + \Gamma_4 \text{diag} \left\{ z_i \tan \left(\frac{\pi z_i}{2} \right) \right\} \mathbf{s} + \left(\frac{\hat{\mathbf{c}}_m^T \Theta}{2\varepsilon_N^2} + \frac{1}{2} \right) \mathbf{s} + \gamma_5 \Omega - \mathbf{f}_{dis} \right\} \\
 &\quad - \tilde{\mathbf{c}}_m^T \left(\frac{\Theta \|\mathbf{s}\|^2}{2\varepsilon_N^2} - \zeta \hat{\mathbf{c}}_m \right) + \Omega^T \dot{\Omega} \\
 &= -G(\mathbf{s}) (\gamma_1 \|\mathbf{s}\|^{\sigma_2+2} + \gamma_2 \|\mathbf{s}\|^{\beta_1+1} + \gamma_3 \|\mathbf{s}\|^2) \\
 &\quad - \mathbf{s}^T \Gamma_4 \text{diag} \left\{ z_i \tan \left(\frac{\pi z_i}{2} \right) \right\} \mathbf{s} - \frac{\hat{\mathbf{c}}_m^T \Theta}{2\varepsilon_N^2} \|\mathbf{s}\|^2 + \mathbf{s}^T \mathbf{f}_{dis} - \frac{\tilde{\mathbf{c}}_m^T \Theta}{2\varepsilon_N^2} \|\mathbf{s}\|^2 \\
 &\quad + \tilde{\mathbf{c}}_m^T \zeta \hat{\mathbf{c}}_m - \frac{1}{2} \mathbf{s}^T \mathbf{s} - \gamma_5 \mathbf{s}^T \Omega + \mathbf{s}^T \mathbf{B}(\mathbf{x}_1) \delta_c + \Omega^T \dot{\Omega}
 \end{aligned} \tag{36}$$

Considering the auxiliary system Equation (32), the above equation leads to

$$\begin{aligned}
 \dot{V}_2 &= -G(\mathbf{s}) (\gamma_1 \|\mathbf{s}\|^{\sigma_2+2} + \gamma_2 \|\mathbf{s}\|^{\beta_1+1} + \gamma_3 \|\mathbf{s}\|^2) \\
 &\quad - \mathbf{s}^T \Gamma_4 \text{diag} \left\{ z_i \tan \left(\frac{\pi z_i}{2} \right) \right\} \mathbf{s} - \frac{\hat{\mathbf{c}}_m^T \Theta}{2\varepsilon_N^2} \|\mathbf{s}\|^2 + \mathbf{s}^T \mathbf{f}_{dis} - \frac{\tilde{\mathbf{c}}_m^T \Theta}{2\varepsilon_N^2} \|\mathbf{s}\|^2 \\
 &\quad + \tilde{\mathbf{c}}_m^T \zeta \hat{\mathbf{c}}_m - \frac{1}{2} \mathbf{s}^T \mathbf{s} - \gamma_5 \mathbf{s}^T \Omega + \mathbf{s}^T \mathbf{B}(\mathbf{x}_1) \delta_c - b_1 \Omega^T \Omega^{1+\sigma_2} \\
 &\quad - b_2 \Omega^T \Omega^{\beta_1} - b_3 \Omega^T \Omega - \|\mathbf{s}^T \mathbf{B}(\mathbf{x}_1) \delta_c\|_1 - \frac{1}{2} b_4 \delta_c^T \delta_c + b_4 \Omega^T \delta_c \\
 &\leq -G(\mathbf{s}) (\gamma_1 \|\mathbf{s}\|^{\sigma_2+2} + \gamma_2 \|\mathbf{s}\|^{\beta_1+1} + \gamma_3 \|\mathbf{s}\|^2) \\
 &\quad - \Gamma_4 \text{diag} \left\{ z_i \tan \left(\frac{\pi z_i}{2} \right) \right\} \|\mathbf{s}\|^2 - \frac{\mathbf{c}_m^T \Theta}{2\varepsilon_N^2} \|\mathbf{s}\|^2 + \mathbf{c}_z^T \theta \|\mathbf{s}\| + \tilde{\mathbf{c}}_m^T \zeta \hat{\mathbf{c}}_m \\
 &\quad - \frac{1}{2} \mathbf{s}^T \mathbf{s} - \gamma_5 \mathbf{s}^T \Omega - b_1 \Omega^T \Omega^{1+\sigma_2} - b_2 \Omega^T \Omega^{\beta_1} - b_3 \Omega^T \Omega \\
 &\quad - \frac{1}{2} b_4 \delta_c^T \delta_c + b_4 \Omega^T \delta_c
 \end{aligned} \tag{37}$$

According to Young’s inequality, for $\forall \lambda_j > \frac{1}{2}$, $j = (1,2,3)$, the following inequality relations hold:

$$\mathbf{c}_z^T \theta \|\mathbf{s}\| = c_1 \|\mathbf{s}\| + c_2 \|\mathbf{x}_1\| \|\mathbf{s}\| + c_3 \|\mathbf{x}_2\|^2 \|\mathbf{s}\| \leq \frac{\mathbf{c}_m^T \Theta}{2\varepsilon_N^2} \|\mathbf{s}\|^2 + \frac{3}{2} \varepsilon_N^2 \tag{38}$$

$$\begin{aligned}
 \tilde{\mathbf{c}}_m^T \zeta \hat{\mathbf{c}}_m &= \sum_{j=1}^3 \zeta_j \tilde{c}_{m_j} \hat{c}_{m_j} = \sum_{j=1}^3 \zeta_j \tilde{c}_{m_j} (c_{m_j} - \tilde{c}_{m_j}) \\
 &\leq \sum_{j=1}^3 \zeta_j \left(\frac{\lambda_j}{2} c_{m_j}^2 - \frac{2\lambda_j - 1}{2\lambda_j} \tilde{c}_{m_j}^2 \right)
 \end{aligned} \tag{39}$$

$$-\gamma_5 \mathbf{s}^T \Omega \leq \frac{1}{2} \mathbf{s}^T \mathbf{s} + \frac{1}{2} \gamma_5^2 \Omega^T \Omega \tag{40}$$

$$\Omega^T \delta_c \leq \frac{1}{2} \Omega^T \Omega + \frac{1}{2} \delta_c^T \delta_c \tag{41}$$

Remark 6. For $z_i = e_{li}/\rho_i$, when $e_{li} < 0$, $z_i < 0$ holds and then $\tan \left(\frac{\pi z_i}{2} \right) < 0$, resulting in $z_i \tan \left(\frac{\pi z_i}{2} \right) > 0$. Similarly, when $e_{li} \geq 0$, $z_i \geq 0$ holds and then $\tan \left(\frac{\pi z_i}{2} \right) \geq 0$, leading to $z_i \tan \left(\frac{\pi z_i}{2} \right) \geq 0$. In summary, $z_i \tan \left(\frac{\pi z_i}{2} \right)$ is consistently non-negative.

Using the above inequalities, Equation (37) can be written as

$$\begin{aligned} \dot{V}_2 \leq & -G(\mathbf{s}) \left(\gamma_1 \|\mathbf{s}\|^{\sigma_2+2} + \gamma_2 \|\mathbf{s}\|^{\beta_1+1} + \gamma_3 \|\mathbf{s}\|^2 \right) \\ & + \frac{3}{2} \epsilon_N^2 + \sum_{j=1}^3 \zeta_j \left(\frac{\lambda_j}{2} c_{m_j}^2 \right) - \sum_{j=1}^3 \zeta_j \left(\frac{2\lambda_j - 1}{2\lambda_j} \tilde{c}_{m_j}^2 \right) \\ & - b_1 \mathbf{\Omega}^T \mathbf{\Omega}^{1+\sigma_2} - b_2 \mathbf{\Omega}^T \mathbf{\Omega}^{\beta_1} - \left(b_3 - \frac{1}{2} \gamma_5^2 - \frac{1}{2} b_4 \right) \mathbf{\Omega}^T \mathbf{\Omega} \end{aligned} \tag{42}$$

Choose parameters b_3, b_4 and γ_5 , such that $b_3 - \frac{1}{2} \gamma_5^2 - \frac{1}{2} b_4 > 0$. Thus, one has

$$\begin{aligned} \dot{V}_2 \leq & -\gamma_1 G(\mathbf{s}) 2^{\frac{\sigma_2+2}{2}} \left(\frac{1}{2} \mathbf{s}^T \mathbf{s} \right)^{\frac{\sigma_2+2}{2}} - \gamma_2 G(\mathbf{s}) 2^{\frac{\beta_1+1}{2}} \left(\frac{1}{2} \mathbf{s}^T \mathbf{s} \right)^{\frac{\beta_1+1}{2}} \\ & - \sum_{j=1}^3 \left(\frac{y_j}{2\eta_j} \tilde{c}_{m_j}^2 \right)^{\frac{\sigma_2+2}{2}} - \sum_{j=1}^3 \left(\frac{y_j}{2\eta_j} \tilde{c}_{m_j}^2 \right)^{\frac{\beta_1+1}{2}} - 2^{\frac{\sigma_2+2}{2}} b_2 \left(\frac{1}{2} \mathbf{\Omega}^T \mathbf{\Omega} \right)^{\frac{\sigma_2+2}{2}} \\ & - 2^{\frac{\beta_1+1}{2}} b_3 \left(\frac{1}{2} \mathbf{\Omega}^T \mathbf{\Omega} \right)^{\frac{\beta_1+1}{2}} + \Delta \end{aligned} \tag{43}$$

where $y_j = \eta_j \zeta_j \frac{2\lambda_j - 1}{2\lambda_j}$, and $\Delta = \sum_{j=1}^3 \left(\frac{y_j}{2\eta_j} \tilde{c}_{m_j}^2 \right)^{\frac{\sigma_2+2}{2}} + \sum_{j=1}^3 \left(\frac{y_j}{2\eta_j} \tilde{c}_{m_j}^2 \right)^{\frac{\beta_1+1}{2}} + \sum_{j=1}^3 \left(\frac{\zeta_j \lambda_j}{2} c_{m_j}^2 \right) - \sum_{j=1}^3 \left(\frac{y_j}{\eta_j} \tilde{c}_{m_j}^2 \right) + \frac{3}{2} \epsilon_N^2$.

If $\frac{y_j}{2\eta_j} \tilde{c}_{m_j}^2 \geq 1$, the following inequality holds

$$\begin{aligned} \left(\frac{y_j}{2\eta_j} \tilde{c}_{m_j}^2 \right)^{\frac{\sigma_2+2}{2}} + \left(\frac{y_j}{2\eta_j} \tilde{c}_{m_j}^2 \right)^{\frac{\beta_1+1}{2}} - \left(\frac{y_j}{\eta_j} \tilde{c}_{m_j}^2 \right) & \leq \left(\frac{y_j}{2\eta_j} \tilde{c}_{m_j}^2 \right)^{\frac{\sigma_2+2}{2}} - \left(\frac{y_j}{2\eta_j} \tilde{c}_{m_j}^2 \right) \\ & \leq \left(\frac{y_j}{2\eta_j} \tilde{c}_{m_j}^2 \right)^{\frac{\sigma_2+2}{2}} - 1 \end{aligned} \tag{44}$$

On the other hand, for the case $\frac{y_j}{2\eta_j} \tilde{c}_{m_j}^2 < 1$, it yields

$$\left(\frac{y_j}{2\eta_j} \tilde{c}_{m_j}^2 \right)^{\frac{\sigma_2+2}{2}} + \left(\frac{y_j}{2\eta_j} \tilde{c}_{m_j}^2 \right)^{\frac{\beta_1+1}{2}} - \left(\frac{y_j}{\eta_j} \tilde{c}_{m_j}^2 \right) \leq \left(\frac{y_j}{2\eta_j} \tilde{c}_{m_j}^2 \right)^{\frac{\beta_1+1}{2}} - \left(\frac{y_j}{2\eta_j} \tilde{c}_{m_j}^2 \right) \leq 1 \tag{45}$$

According to the theory of uniform boundedness, \mathbf{s} and $\tilde{\mathbf{c}}_m$ are uniformly bounded. Therefore, there are always some positive constants $\vartheta_j (j = 1, 2, 3)$ such that $|\tilde{c}_{m_j}| < \vartheta_j$. Then,

$$\begin{aligned} \Delta & = \sum_{j=1}^3 \left\{ \left(\frac{y_j}{2\eta_j} \tilde{c}_{m_j}^2 \right)^{\frac{\sigma_2+2}{2}} + \left(\frac{y_j}{2\eta_j} \tilde{c}_{m_j}^2 \right)^{\frac{\beta_1+1}{2}} - \left(\frac{y_j}{\eta_j} \tilde{c}_{m_j}^2 \right) \right\} \\ & + \sum_{j=1}^3 \left(\frac{\zeta_j \lambda_j}{2} c_{m_j}^2 \right) + \frac{3}{2} \epsilon_N^2 \\ & \leq \sum_{j=1}^3 \max \left\{ \left(\frac{y_j}{2\eta_j} \vartheta_j^2 \right)^{\frac{\sigma_2+2}{2}} - 1, 1 \right\} + \sum_{j=1}^3 \left(\frac{\zeta_j \lambda_j}{2} c_{m_j}^2 \right) + \frac{3}{2} \epsilon_N^2 < \infty \end{aligned} \tag{46}$$

Using Lemma 1, the previous inequality Equation (43) is further simplified as

$$\begin{aligned} \dot{V}_2 &\leq -\gamma_1 G(\mathbf{s}) 2^{\frac{\sigma_2+2}{2}} \left(\frac{1}{2} \mathbf{s}^T \mathbf{s}\right)^{\frac{\sigma_2+2}{2}} - y_m \left(\frac{1}{2} \tilde{\mathbf{c}}_m^T \boldsymbol{\eta}^{-1} \tilde{\mathbf{c}}_m\right)^{\frac{\sigma_2+2}{2}} \\ &\quad - 2^{\frac{\sigma_2+2}{2}} b_2 \left(\frac{1}{2} \boldsymbol{\Omega}^T \boldsymbol{\Omega}\right)^{\frac{\sigma_2+2}{2}} - \gamma_2 G(\mathbf{s}) 2^{\frac{\beta_1+1}{2}} \left(\frac{1}{2} \mathbf{s}^T \mathbf{s}\right)^{\frac{\beta_1+1}{2}} \\ &\quad - y_m \left(\frac{1}{2} \tilde{\mathbf{c}}_m^T \boldsymbol{\eta}^{-1} \tilde{\mathbf{c}}_m\right)^{\frac{\beta_1+1}{2}} - 2^{\frac{\beta_1+1}{2}} b_3 \left(\frac{1}{2} \boldsymbol{\Omega}^T \boldsymbol{\Omega}\right)^{\frac{\beta_1+1}{2}} + \Delta \\ &\leq -a V_2^{\frac{\sigma_2+2}{2}} - b V_2^{\frac{\beta_1+1}{2}} + \Delta \end{aligned} \tag{47}$$

where $y_m = \min \left\{ y_1^{\frac{\sigma_2+2}{2}}, y_2^{\frac{\sigma_2+2}{2}}, y_3^{\frac{\sigma_2+2}{2}} \right\}$, $a = 3^{-\frac{\sigma_2}{2}} \min \left\{ 2^{\frac{\sigma_2+2}{2}} \gamma_1 G(\mathbf{s}), y_m, 2^{\frac{\sigma_2+2}{2}} b_2 \right\}$, $b = \min \left\{ 2^{\frac{\beta_1+1}{2}} \gamma_2 G(\mathbf{s}), y_m, 2^{\frac{\beta_1+1}{2}} b_3 \right\}$.

Therefore, according to Lemma 3, it can be concluded that the NFTSS (13) is practically fixed-time stable and converges to the following residual set Π after a bounded time T_r .

$$\Pi := \left\{ \lim_{t \rightarrow T_r} \mathbf{s}(t) \mid \|\mathbf{s}(t)\| \leq \Phi \right\} \tag{48}$$

where for $0 < o_1, o_2 \leq 1$,

$$\Phi = \min \left\{ \left(\frac{\Delta}{a(1-o_1)} \right)^{\frac{2}{\sigma_2+2}}, \left(\frac{\Delta}{b(1-o_2)} \right)^{\frac{2}{\beta_1+1}} \right\} \tag{49}$$

$$T_r = \frac{2}{a\sigma_2} + \frac{2}{b(1-\beta_1)} \tag{50}$$

Step 2. Once \mathbf{s} reaches the region Π , the fixed-time convergence property of the system states should be demonstrated by the following analysis.

Case 1. If $\mathbf{s} = 0$ is reached, then $\bar{s}_i = 0$. Based on Lemma 4, the fixed-time convergence of tracking error \mathbf{e}_1 and velocity error \mathbf{e}_2 can be guaranteed during the sliding phase.

Case 2. In the case of $\bar{s}_i \neq 0$ and $|e_{1i}| \geq \varepsilon_0$, let $s_i = \phi_i \in \Pi$ and one has

$$s_i = e_{2i} + N(\mathbf{e}_1) \left(K_{1i} \text{sig}^{1+\sigma_1}(e_{1i}) + K_{2i} \text{sig}^{\frac{p}{q}}(e_{1i}) \right) = \phi_i \tag{51}$$

it follows that

$$\begin{aligned} e_{2i} + N(\mathbf{e}_1) \left(K_{1i} - \frac{\phi_i}{N(\mathbf{e}_1) \text{sig}^{1+\sigma_1}(e_{1i})} \right) \text{sig}^{1+\sigma_1}(e_{1i}) \\ + N(\mathbf{e}_1) K_{2i} \text{sig}^{\frac{p}{q}}(e_{1i}) = 0 \end{aligned} \tag{52}$$

$$\begin{aligned} e_{2i} + N(\mathbf{e}_1) K_{1i} \text{sig}^{1+\sigma_1}(e_{1i}) \\ + N(\mathbf{e}_1) \left(K_{2i} - \frac{\phi_i}{N(\mathbf{e}_1) \text{sig}^{\frac{p}{q}}(e_{1i})} \right) \text{sig}^{\frac{p}{q}}(e_{1i}) = 0 \end{aligned} \tag{53}$$

Choosing K_{1i} such that $K_{1i} - \frac{\phi_i}{N(\mathbf{e}_1) \text{sig}^{1+\sigma_1}(e_{1i})} > 0$ or $K_{2i} - \frac{\phi_i}{N(\mathbf{e}_1) \text{sig}^{\frac{p}{q}}(e_{1i})} > 0$, then the fixed-time stability of the system can still be guaranteed. Therefore, the tracking error e_{1i} ultimately converges

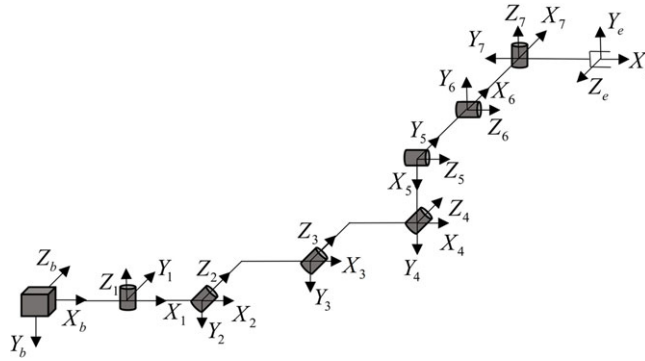


Figure 4. D-H model of the studied space manipulator system.

to the region $|e_{1i}| \leq \Psi_{e1}$ after a fixed time. At this time, it is easy to derive that the tracking velocity e_{2i} converges to the region $|e_{2i}| \leq \Psi_{e2}$ after a fixed time.

Case 3. For the case $\bar{s}_i \neq 0$ and $|e_{1i}| < \varepsilon_0$. Since the tracking error e_{1i} has entered the region Ψ_{e1} , according to the NFTSS (13), one obtains

$$s_i = e_{2i} + N(\mathbf{e}_1) (K_{1i} \text{sig}^{1+\sigma_1}(e_{1i}) + K_{2i} (l_1 e_{1i} + l_2 e_{1i}^2 \text{sgn}(e_{1i}))) = \phi_i \tag{54}$$

It follows that

$$|e_{2i}| \leq \phi_i + N(\mathbf{e}_1) (K_{1i} |e_{1i}|^{1+\sigma_1} + K_{2i} |l_1 e_{1i} + l_2 e_{1i}^2 \text{sgn}(e_{1i})|) \leq \Psi_{e2} \tag{55}$$

The above analysis shows that the system states e_{1i} and e_{2i} will converge to the sets $|e_{1i}| \leq \Psi_{e1}$ and $|e_{2i}| \leq \Psi_{e2}$ after a fixed time, respectively. It is concluded that the closed-loop tracking control system is practically fixed-time stable. The proof is completed.

Remark 7. Appropriate control parameters are crucial for achieving improved control accuracy when adopting the suggested control scheme into practice. Therefore, here are some suggestions for parameter selection:

- (a) According to Equation (14), the selection of ε_0 will have a direct impact on the effectiveness of the singularity problem solution, directly affecting the convergence accuracy of the system state.
- (b) Larger K_{1i} and K_{2i} will result in a faster convergence rate at the cost of more control energy consumption in the initial response, especially when the initial state is far from the equilibrium point.
- (c) For the purpose of tracking control with high precision, ε_N should be selected small enough, which leads to a greater control input. Therefore, a trade-off between the control effort and the system performance is required.
- (d) Unexpected changes in the control inputs may have a negative effect on the actuator. The influence of the actuator saturation on the auxiliary system can be mitigated by adjusting the value of the parameter b_4 , particularly in cases when the actuator saturation is significant.
- (e) The settling time expression Equation (21) indicates that the parameters q, p, n_1 and m_1 are also crucial in dominating the convergence rate and accuracy.

4.0 Numerical simulations

In this section, numerical simulations of a seven-degrees-of-freedom free-floating space manipulator system are conducted in two parts to evaluate the performance of the proposed adaptive fixed-time control strategy. The D-H model and physical parameters of the studied system are shown in Fig. 4

Table 1. Physical parameters of the studied space manipulator

Parameter	B ₀	B ₁	B ₂	B ₃	B ₄	B ₅	B ₆	B ₇	
mass (kg)	100	4.25	7	7	4.25	4.25	4.25	4.25	
b _i (m)	0.6	0.3	0.25	0.25	-0.25	0.25	0.25	0.3	
a _i (m)	0	0	0	0	0	0	0	0	
	0	0	0.25	0.25	0	0	0	0	
	0	0.3	0.25	0.25	-0.25	0.25	0.25	0.3	
I _i (kg · m ²)	I _{xx} I _{yy} I _{zz} I _{xy} I _{xz} I _{yz}	0	0	0	0	0	0	0	
		0	0	0.25	0.25	0	0	0	
		2,000	0.05	0.09	0.09	0.05	0.05	0.05	1.28
		2,000	1.28	1.46	1.46	0.89	0.89	0.89	1.28
		2,000	1.28	1.46	1.46	0.89	0.89	0.89	0.05
		0	0	0	0	0	0	0	0
		0	0	0	0	0	0	0	0

and Table 1, respectively. In this simulation, considering the system uncertainties, the nominal mass values of the system are set as $m_{B0} = 90$ kg, $m_{B1} = 3.825$ kg, $m_{B2} = 6.3$ kg, $m_{B3} = 6.3$ kg, $m_{B4} = 3.825$ kg, $m_{B5} = 3.825$ kg, $m_{B6} = 3.825$ kg and $m_{B7} = 3.825$ kg. And the time-varying disturbances acted on the system are given by $\mathbf{d}(t) = [0.03\sin(t) + 0.005\sin(200\pi t), 0.03\sin(2t) + 0.005\sin(200\pi t), 0.01\sin(t) + 0.002\sin(200\pi t), 0.01\sin(2t) + 0.001\sin(200\pi t), 0.02\sin(t) + 0.002\sin(200\pi t), 0.01\sin(3t) + 0.001\sin(200\pi t), 0.02\sin(3t) + 0.003\sin(200\pi t)]^T$ N · m. The initial state of the spacecraft base is chosen as $[0, 0, 0, 1, 0, 0, 0]^T$. The joint initial and desired configurations are assigned as $[0, \pi/3, 0, \pi/4, \pi/4, 0, \pi/6]^T$ rad and $[0.15 - 0.14e^{-t} + 0.07e^{-2t}, 1.05 + 0.1e^{-t} - 0.05e^{-2t}, s0.17 + 0.1e^{-2t} - 0.2e^{-t}, 0.48 - 0.1e^{-3t} + 0.3e^{-t}, 0.8 - 0.05e^{-2t} + 0.1e^{-t}, -0.2 + 0.2e^{-t} - 0.1e^{-2t}, 0.7 + 0.25e^{-2t} - 0.5e^{-t}]^T$ rad. The parameters of the prescribed performance boundary are set as $\rho_0 = 0.15$, $\rho_\infty = 5 \times 10^{-6}$, and $l_0 = 2.5$. The controller parameters are listed in Table 2.

4.1 Performance evaluation with healthy actuators

In this part, the input saturation is ignored, and the main purpose is to investigate the effect of the PPC constraint on the tracking performance. The proposed control scheme is compared with an adaptive fixed-time sliding mode controller (AFSMTC) that does not take into account performance constraints. The AFSMTC has the same form as the proposed scheme, except for the tan-type PPC term. For a fair comparison, the control parameters chosen for the AFSMTC are identical to those of the proposed scheme. The simulation results are given in Figs 5–8.

Figures 5–7 illustrate the time responses of the position and velocity tracking errors. These results validate the stability analysis in Section 3 comfortably. Although both controllers enable fixed-time convergence, the proposed controller possesses a faster transient response with higher steady-state accuracy. Furthermore, with the help of tan-type PPC, the position tracking errors are always strictly limited to the predefined boundary in both transient and steady-state phases, whereas those of the AFSMTC violate the constraint. As can be seen, since the constraint boundary is decaying with time, the norm of tracking error is decreasing, which increases the tracking precision. It is the effect of the prescribed performance function in the proposed control scheme. Control torques are depicted in Fig. 8, from which the maximum torque required by the proposed controller is slightly larger than that of the AFSMTC. This is because the control gain is increased to counteract the evolution of the tracking error when it approaches the constraint boundary. It is worth noting that to obtain fast trajectory tracking, both controllers have a large transient response at the beginning of the movement, which can make them impossible for practical applications. Therefore, the influence of actuator saturation needs to be considered during the controller design process.

Table 2. Parameters of the proposed controller

Parameter	Values
Positive integer m_1	9
Positive integer n_1	7
Positive odd integer p	11
Positive odd integer q	13
Positive constant ε_0	0.001
Positive constant ε_N	0.4
Positive definite matrix \mathbf{K}_1	diag (1.5, 1.8, 1.5, 1.6, 1.8, 1.8, 1.2)
Positive definite matrix \mathbf{K}_2	diag (0.8, 1.2, 1.2, 1.0, 0.8, 1.0, 1.2)
Positive constant s_m	5
Positive constant s_n	2
Positive constant s_r	3
Positive constant α_1	$\frac{9}{7}$
Positive constant β_1	$\frac{9}{13}$
Control gain γ_1	0.8
Control gain γ_2	0.5
Control gain γ_3	0.5
Control gain γ_5	0.1
Gain parameter χ	0.3
Gain parameter v_1	5
Gain parameter k	3
Control gain matrix Γ_4	diag(1.2,2.5,3,2.2,2,1.8,2.2)
Adaptive gain matrix	diag (0.8, 0.8, 2)
Adaptive gain matrix	diag (0.01, 0.01, 0.01)
Auxiliary system constant b_1	1
Auxiliary system constant b_2	0.5
Auxiliary system constant b_3	2.2
Auxiliary system constant b_4	0.15
Auxiliary system constant Ω_0	0.0001

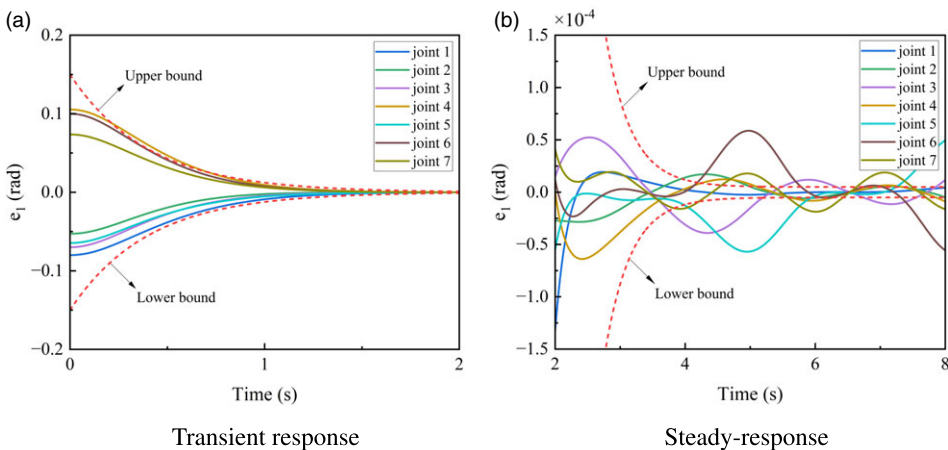


Figure 5. Time response of position tracking error under the AFSMTC.

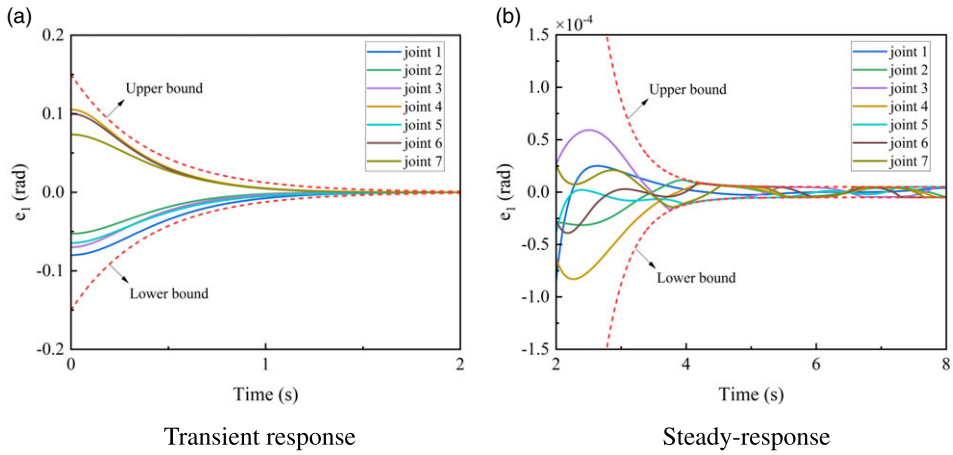


Figure 6. Time response of position tracking error under the proposed controller.

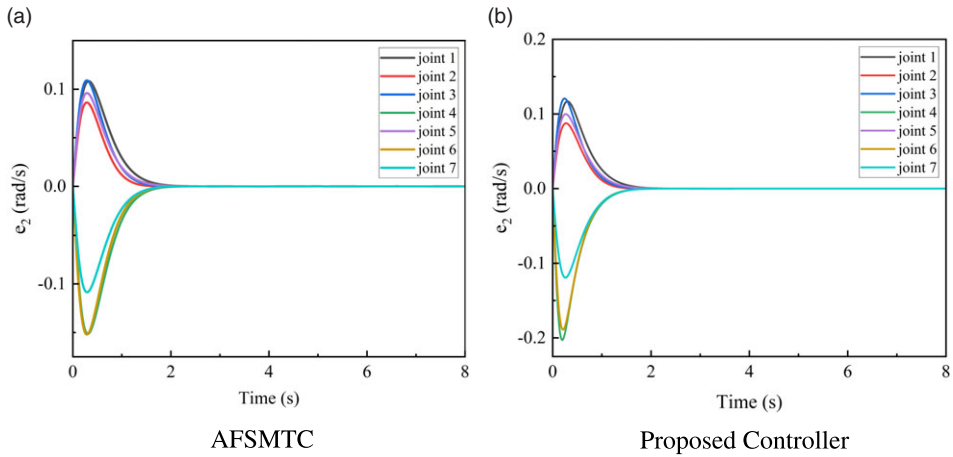


Figure 7. Time response of velocity tracking error.

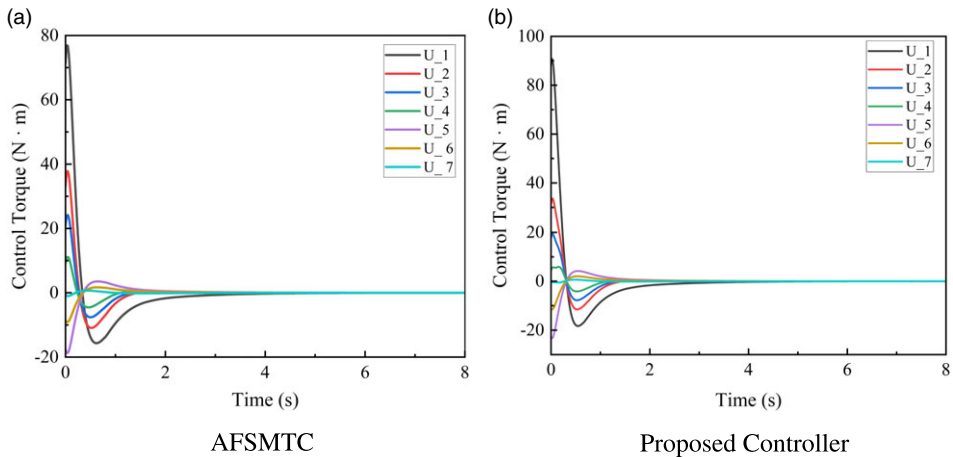


Figure 8. Time response of control torques.

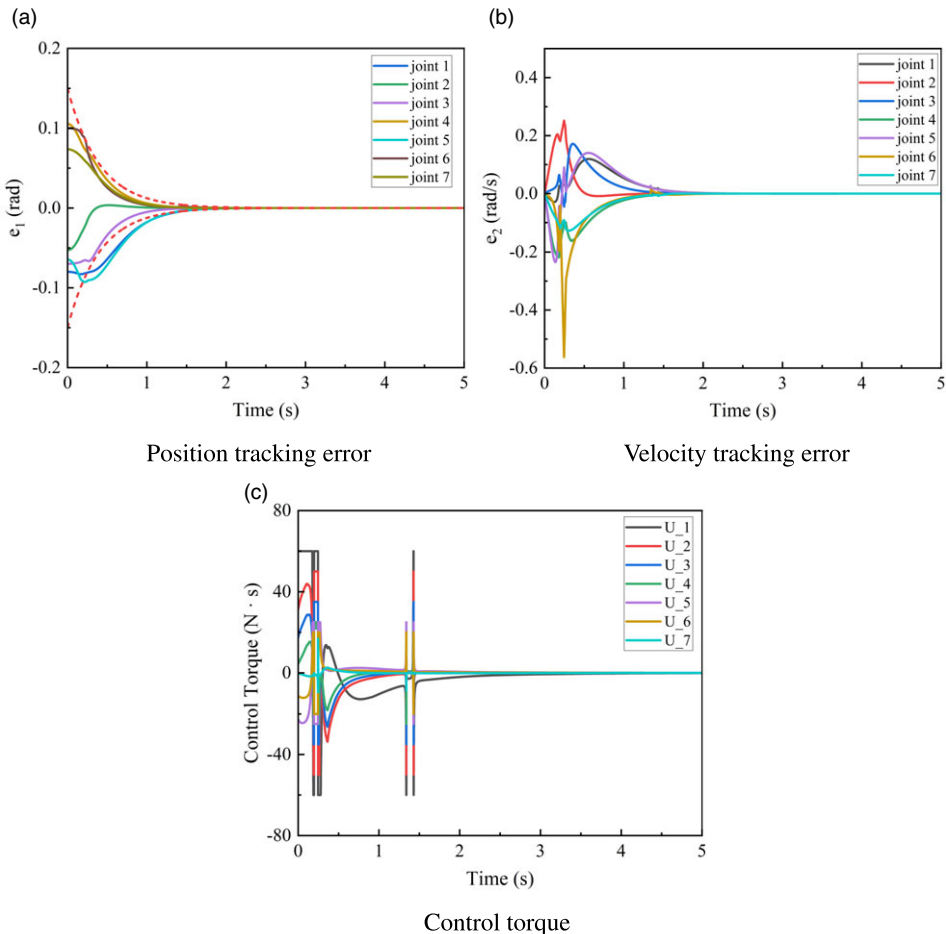


Figure 9. Simulation results without the saturation compensator.

4.2 Performance evaluation with input saturation

In this part, the problem of input saturation is investigated and the capability of the proposed controller is evaluated in the following two simulation sections. To this end, the allowable maximum input control torques are selected as $[60, 50, 35, 25, 25, 20, 30]^T \text{N} \cdot \text{m}$.

4.2.1 Performance validation of the saturation compensator

In this simulation, the main objective is to illustrate the effectiveness of the proposed saturation compensator in the proposed control method, two cases are discussed for comparison. One is the tracking control with saturation compensation, and the other is the tracking control without saturation compensation.

The simulation results without and with saturation compensation are presented in Figs 9 and 10, respectively. As shown in Fig. 9, the convergence time of tracking error and tracking speed error is finite, but the error constraint boundary is no longer satisfied. It indicates that input saturation has greatly attenuated the convergence performance of trajectory tracking. From Fig. 10, the predicted compensation parameter Ω converges quickly to a constant, which means a strong compensation role when starting to track the desired trajectory. Under the action of the saturation compensator, the tracking error is not only always strictly remained within the predefined constraint bounds, but also a superior control performance is obtained with shorter settling time and faster convergence speed. By comparison, the actual control torques for both controllers are guaranteed to be within their maximum allowable limits. It should be noted that due to the influence of input saturation, the torque produces a strong chattering phenomenon.

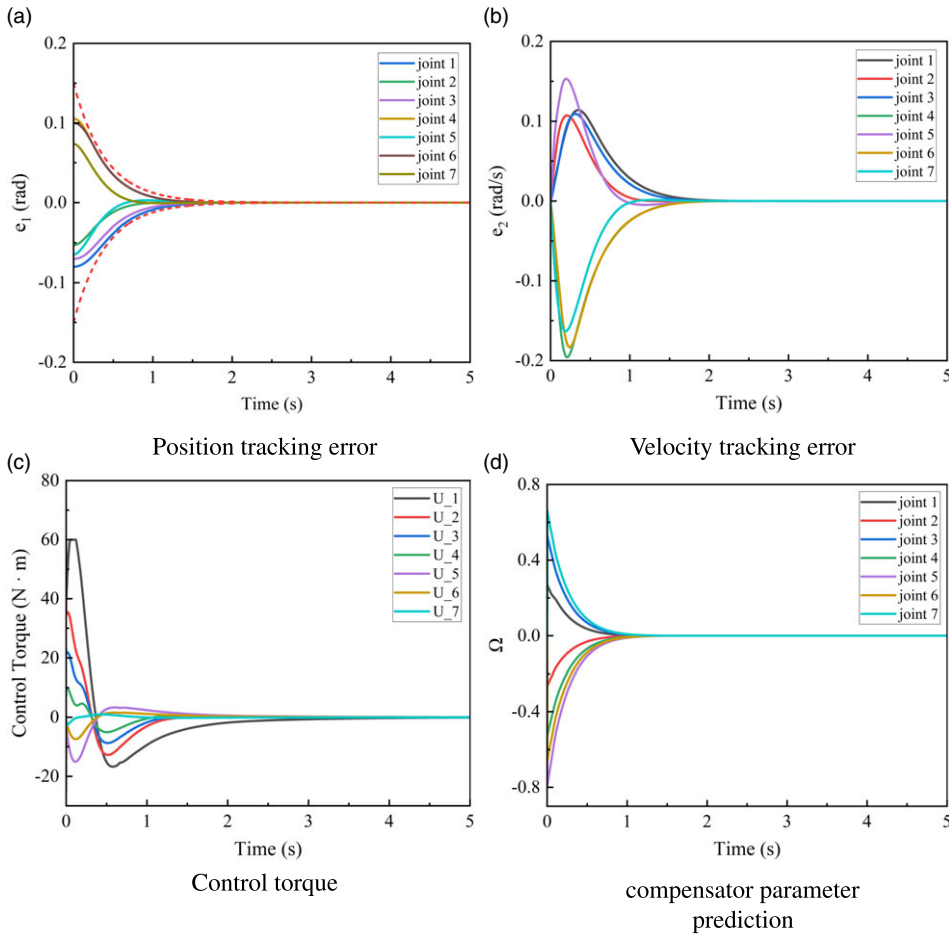


Figure 10. Simulation results with the saturation compensator.

Whereas with the help of the saturation compensator, the control torque obtained is smoother with significantly less chattering. To sum up, conclusions can be drawn the proposed saturation compensator can eliminate the effect of input saturation to a certain extent and accelerate the convergence rate of trajectory tracking in the proposed control scheme.

4.2.2 Performance comparison with existing methods

To further assess the proposed controller’s performance, comparisons are performed with the existing fixed-time control strategies proposed in Refs [18, 47]. To ensure the rationality of the comparison, all simulation experiments are conducted under the same initial conditions. The FTSMC can be described as follows [18]:

$$\begin{aligned}
 \mathbf{u} &= \mathbf{u}_1 + \mathbf{u}_2 + \mathbf{u}_3 \\
 \mathbf{u}_1 &= -\mathbf{B}^{-1}(\mathbf{x}_1) (\mathbf{F}(\mathbf{x}_1, \mathbf{x}_2) - \ddot{\mathbf{q}}_d) \\
 &\quad - \mathbf{B}^{-1}(\mathbf{x}_1) \sigma^{-1} \Phi \mathbf{e}_2 - \frac{P_1}{q_1} (\sigma \mathbf{B}(\mathbf{x}_1))^{-1} \text{diag}(|\sigma \mathbf{e}_2|^{1-q_1/p_1}) \mathbf{e}_2 \\
 \mathbf{u}_2 &= -\frac{P_1}{q_1} (\sigma \mathbf{B}(\mathbf{x}_1))^{-1} \text{diag}(\text{sig}^{2-q_1/p_1}(\sigma \mathbf{e}_2)) \mu_\tau \\
 &\quad (\alpha_2 \text{sig}^{m_2/n_2}(\mathbf{s}) + \beta_2 \text{sig}^{p_2/q_2}(\mathbf{s})) \\
 \mathbf{u}_3 &= -\mathbf{B}^{-1}(\mathbf{x}_1) (c_1 + c_2 \|\mathbf{x}_1\| + c_3 \|\mathbf{x}_2\|^2) \frac{\mathbf{s}}{\|\mathbf{s}\|} \\
 \mathbf{s} &= \mathbf{e}_1 + \text{sig}^{q_1/p_1}(\sigma \mathbf{e}_2)
 \end{aligned}
 \tag{56}$$

Table 3. Controller parameters for FTSMC and ANFTSMC

Controllers	Parameters
FTSMC	$\alpha_1 = [0.5, 0.6, 0.5, 0.6, 1.2, 0.8, 0.8]$, $\beta_1 = [0.8, 1.2, 1.2, 1.0, 0.8, 1.0, 1.2]$, $m_1 = 9, n_1 = 5, p_1 = 7, q_1 = 9, m_2 = 5,$ $n_2 = 3, p_2 = 5, q_2 = 9, \alpha_2 = 2, \beta_2 = 2,$ $c_1 = 0.2, c_2 = 0.1, c_3 = 0.1$
ANFTSMC	$\mathbf{K}_a = \text{diag} (0.6, 0.8, 1.0, 0.8, 1.6, 0.8, 1.2),$ $\mathbf{K}_b = \text{diag} (0.6, 0.8, 0.8, 0.6, 1.0, 0.8, 1.2)$ $m_1 = 9, n_1 = 7, p_1 = 11, q_1 = 13, m_2 = 9$ $n_2 = 7, p_2 = 9, q_2 = 13, \alpha_2 = 0.8, \beta_2 = 0.5$ $\eta_{11} = 1.8, \eta_{12} = 1.5, \eta_{13} = 5, \eta_{21} = 0.01,$ $\eta_{22} = 0.01, \eta_{23} = 0.01, \varepsilon = 0.01$

where $\alpha_2 > 0, \beta_2 > 0, c_1, c_2, c_3$ are three positive constants, $\sigma = \text{diag} (\sigma_1, \sigma_2, \dots, \sigma_n)$ with $\sigma_i = \frac{1}{\alpha_1(i)e_i^{m_1/n_1 - p_1/q_1 + \beta_1(i)}}$, $\alpha_1 = [\alpha_{11}, \alpha_{12}, \dots, \alpha_{1n}]$ and $\beta_1 = [\beta_{11}, \beta_{12}, \dots, \beta_{1n}]$ with $\alpha_{1i} > 0$ and $\beta_{1i} > 0$, $\Phi = \text{diag} (\Phi_1, \Phi_2, \dots, \Phi_n)$ with $\Phi_i = -\alpha_{1i} \left(\frac{m_1}{n_1} - \frac{p_1}{q_1} \right) e_i^{m_1/n_1 - p_1/q_1 - 1} \sigma_i^2 e_{2i}$, $m_1, m_2, n_1, n_2, p_1, p_2, q_1, q_2$ are positive odd integers satisfying $m_1 > n_1, m_2 > n_2, p_1 < q_1 < 2p_1, p_2 < q_2$ and $m_1/n_1 - p_1/q_1 > 1$. $\mu_\tau = \text{diag} (\mu_{\tau 1}, \mu_{\tau 2}, \dots, \mu_{\tau n})$ with $\mu_{\tau i}$ given by:

$$\mu_{\tau i} = \begin{cases} \sin \left(\frac{\pi}{2} \cdot \frac{e_{2i}^{q_1/p_1 - 1}}{\tau_i} \right) & \text{if } e_{2i}^{q_1/p_1 - 1} \leq \tau_i \\ 1 & \text{otherwise} \end{cases} \tag{57}$$

The value of $\mu_{\tau i}$ is 1 as the initial tracking speed $\mathbf{e}_2(0) = 0$.

The adaptive nonsingular fast terminal sliding mode control (ANFTSMC) scheme proposed by Ref. [47] is written as

$$\begin{aligned} \mathbf{u} &= \mathbf{u}_1 + \mathbf{u}_2 + \mathbf{u}_3 \\ \mathbf{u}_1 &= -\mathbf{B}^{-1}(\mathbf{x}_1) (\mathbf{F}(\mathbf{x}_1, \mathbf{x}_2) - \ddot{\mathbf{q}}_d) \\ &\quad - \mathbf{B}^{-1}(\mathbf{x}_1) (k_1 \mathbf{K}_a \text{diag}(|e_{1i}|^{k_1 - 1}) \mathbf{e}_2 + \mathbf{K}_b \dot{\mathbf{s}}_\rho(\mathbf{e}_1)) \\ \mathbf{u}_2 &= -\mathbf{B}^{-1}(\mathbf{x}_1) (\alpha_2 \text{sig}^{k_2}(\mathbf{s}) + \beta_2 \text{sig}^{p_2/q_2}(\mathbf{s})) \\ \mathbf{u}_3 &= -\mathbf{B}^{-1}(\mathbf{x}_1) (\hat{c}_1 + \hat{c}_2 \|x_1\| + \hat{c}_3 \|\mathbf{x}_2\|^2) \tanh(s/\varepsilon) \\ \dot{\hat{c}}_1 &= \eta_{11} (s^T \tanh(s/\varepsilon) - \eta_{21} \hat{c}_1) \\ \dot{\hat{c}}_2 &= \eta_{12} (\|x_1\| s^T \tanh(s/\varepsilon) - \eta_{22} \hat{c}_2) \\ \dot{\hat{c}}_3 &= \eta_{13} (\|x_2\|^2 s^T \tanh(s/\varepsilon) - \eta_{23} \hat{c}_3) \\ \mathbf{s} &= \mathbf{e}_2 + \mathbf{K}_a \text{sig}^{k_1}(\mathbf{e}_1) + \mathbf{K}_b \mathbf{s}_\rho(\mathbf{e}_1) \end{aligned} \tag{58}$$

where $\mathbf{K}_a, \mathbf{K}_b$ are positive definite matrices, $\alpha_2 > 0, \beta_2 > 0, k_1 = \frac{1}{2} + \frac{m_1}{2n_1} + \left(\frac{m_1}{2n_1} - \frac{1}{2} \right) \text{sign}(\|\mathbf{e}_1 - 1\|)$, $k_2 = \frac{1}{2} + \frac{m_2}{2n_2} + \left(\frac{m_2}{2n_2} - \frac{1}{2} \right) \text{sign}(\|\mathbf{s} - 1\|)$, m_1, m_2, p_1 and p_2 are positive odd integers satisfying $m_1 > n_1, m_2 > n_2$ and $p_2 < q_2$, $\tanh\left(\frac{s}{\varepsilon}\right) = [\tanh\left(\frac{s_1}{\varepsilon}\right), \tanh\left(\frac{s_2}{\varepsilon}\right), \dots, \tanh\left(\frac{s_n}{\varepsilon}\right)]^T$ with ε is a arbitrary small positive constant, η_{ij} and η_{2j} are positive constants.

Generally, the faster the system responses, the larger control torques generates, resulting in more energy consumption. Therefore, the selection of control parameters requires a trade-off between control performances and input torques. The control parameters for FTSMC and ANFTSMC are listed in Table 3. Figures 11–12 give the response curves of the position and speed tracking errors under these different controllers. The convergence time of all controllers is observed to be bounded, and the suggested

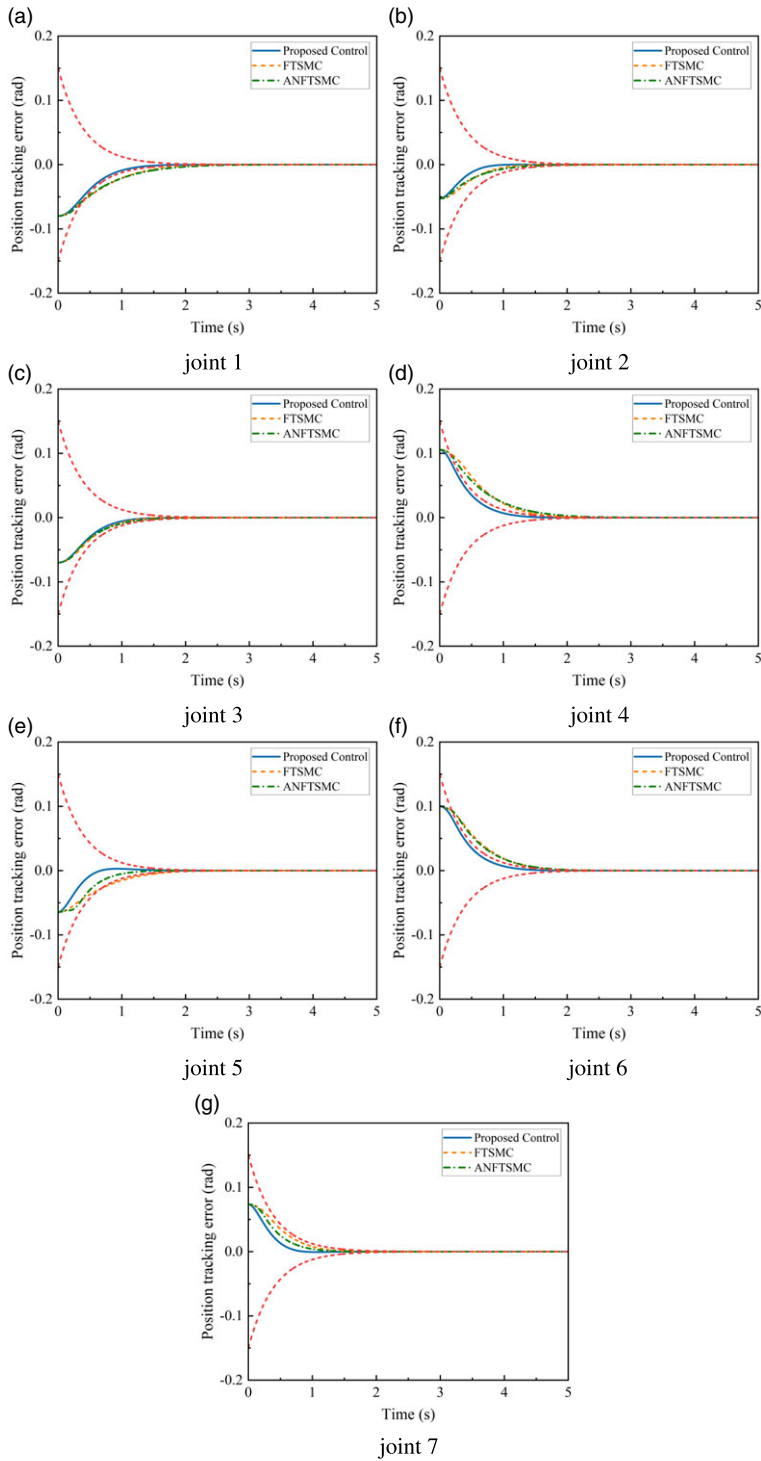


Figure 11. Position tracking error performance.

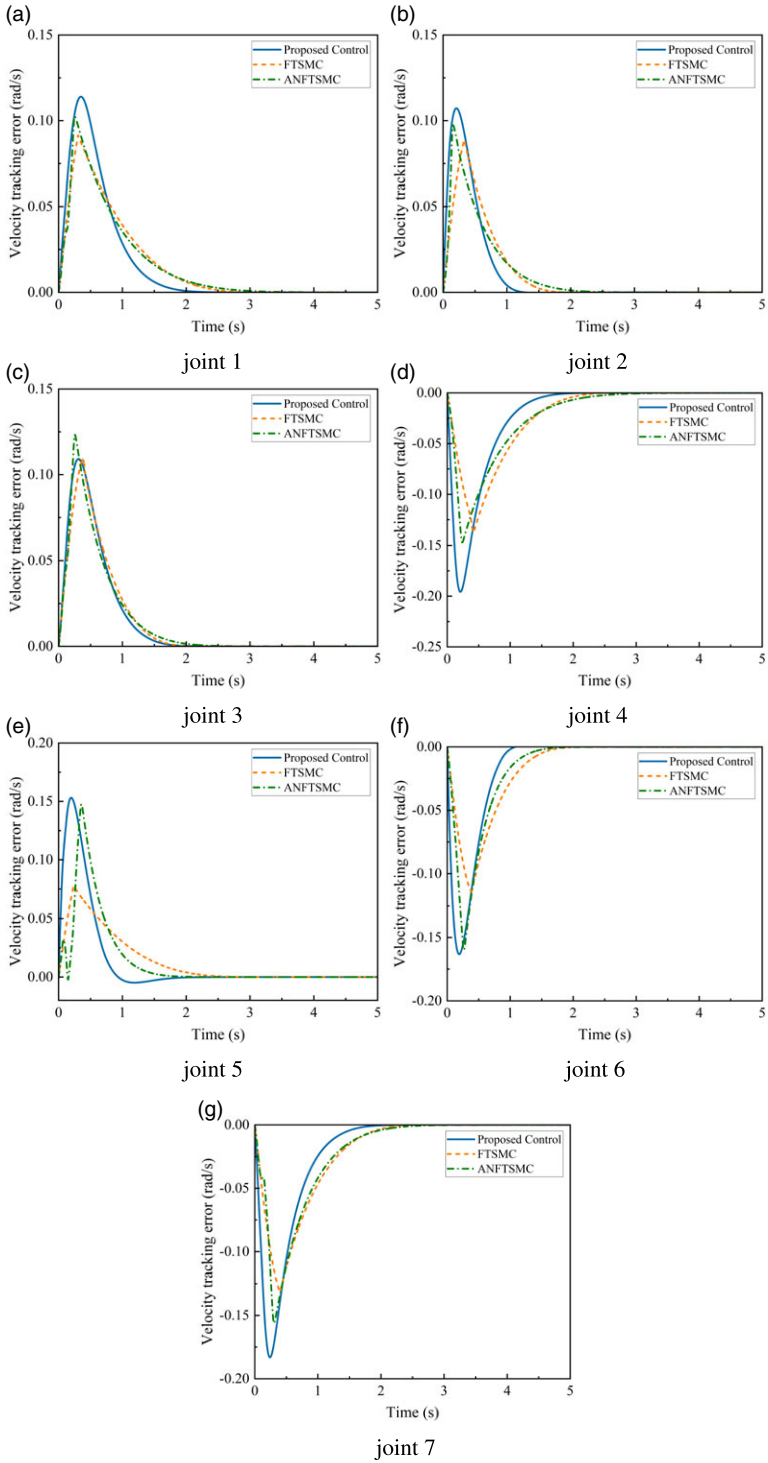


Figure 12. Velocity tracking error performance.

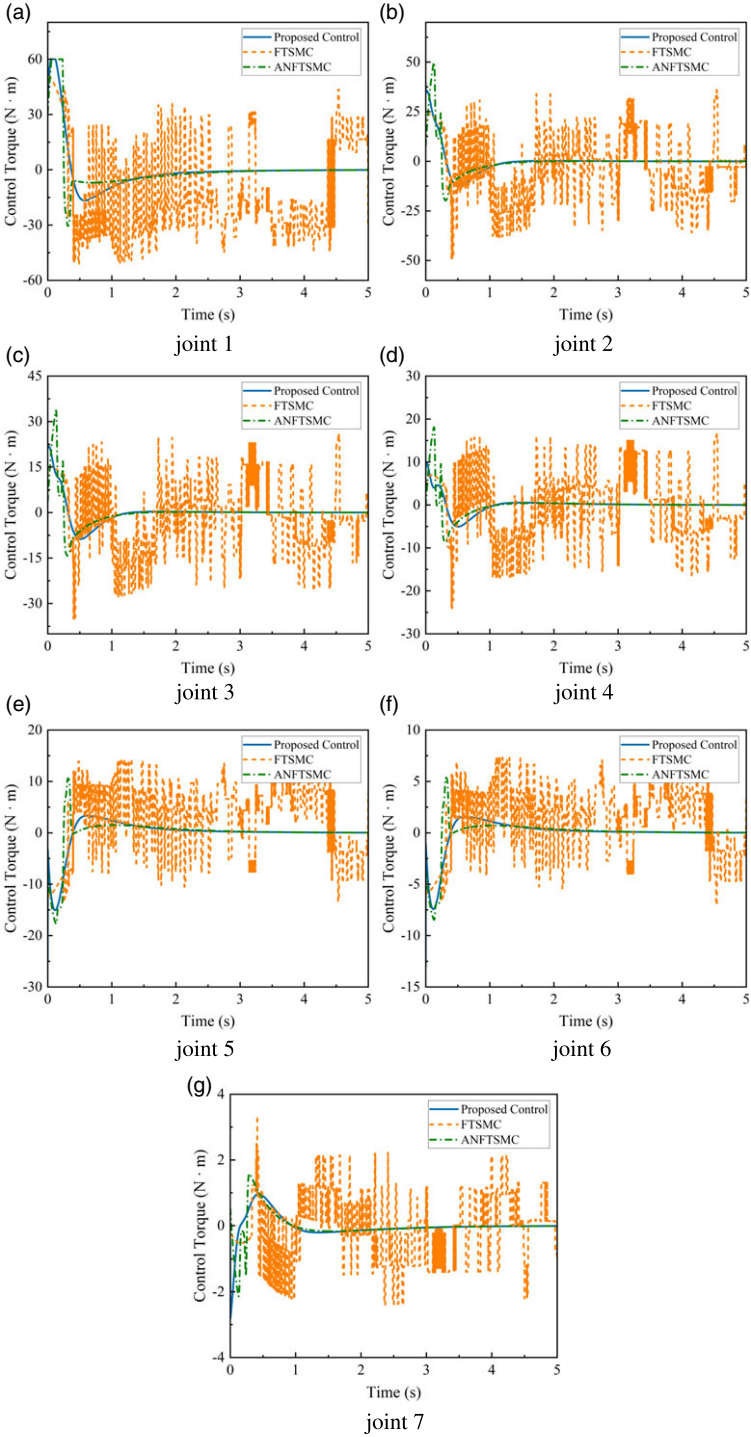


Figure 13. Control torque.

Table 4. IAE index comparison of different controllers

IAE	Proposed controller	FTSMC	ANFTSMC
IAE _{e₁₁}	44.6329	59.8012	61.2166
IAE _{e₁₂}	18.7291	27.4211	28.3564
IAE _{e₁₃}	35.7641	39.0169	39.6325
IAE _{e₁₄}	46.7035	72.8579	73.2816
IAE _{e₁₅}	20.7131	45.1611	35.2228
IAE _{e₁₆}	46.0976	66.0547	65.6735
IAE _{e₁₇}	23.8957	40.8324	33.5227

Table 5. ITAE index comparison of different controllers

ITAE	Proposed controller	FTSMC	ANFTSMC
ITAE _{e₁₁}	17.3168	32.2647	36.1364
ITAE _{e₁₂}	4.6532	9.6328	11.9463
ITAE _{e₁₃}	12.6477	14.6702	16.5088
ITAE _{e₁₄}	15.6069	34.4396	39.6196
ITAE _{e₁₅}	5.6454	23.233	12.2935
ITAE _{e₁₆}	15.5378	30.2576	31.1518
ITAE _{e₁₇}	5.5794	15.2854	10.6605

Table 6. EC index comparison of different controllers

ITAE	Proposed controller	FTSMC	ANFTSMC
ITAE _{e₁₁}	845,770	4,153,800	901,320
ITAE _{e₁₂}	211,200	1,400,400	283,810
ITAE _{e₁₃}	82,180	713,900	127,840
ITAE _{e₁₄}	17,180	302,300	37,020
ITAE _{e₁₅}	48,370	291,900	59,980
ITAE _{e₁₆}	11,290	66,700	13,730
ITAE _{e₁₇}	660	4,500	800

controller takes less time to track the desired trajectory than the other two controllers. Meanwhile, the transient performance requirement is consistently guaranteed only under the proposed control, implying that a quicker convergence performance is realised. Figure 13 clearly depicts the comparison of joint torques. In the presence of input saturation, the proposed controller provides a smoother, more continuous and less chattering control input.

To quantitatively evaluate the performance of the various controllers, for the total number of sampling times N , three metrics including the integrated absolute error (IAE) $IAE_{e_{1i}} = \frac{1}{N} \sum_{j=1}^N |e_{1i}(j)|$, the integrated time absolute error (ITAE) $ITAE_{e_{1i}} = \frac{1}{N} \sum_{j=1}^N t(j) |e_{1i}(j)|$, and the energy consumption (EC) $EC_{u_i} = \frac{1}{N} \sum_{j=1}^N |\tau_i(j)|$ are introduced, as shown in Tables 4–6.

The lower the values of the above three indicators, the better the control performance of the closed-loop tracking system. According to the comparison, the proposed control method can achieve faster tracking convergence and higher tracking precision with less energy consumption than the other two referenced methods. The simulation results demonstrate the noticeable superiority of the proposed controller in terms of tracking performance, energy consumption and chattering suppression.

In summary, it can be concluded that the proposed controller realises fast and accurate trajectory tracking of the space manipulator in a bounded time, while satisfying the transient and steady-state

performance constraints of tracking error, even in the presence of unknown disturbances, inertial uncertainty and input saturation.

5.0 Conclusion

The tracking control issue for a free-floating space manipulator with prescribed performance constraints was addressed in this study, along with an efficient solution taking into account model uncertainties, internal disturbances and input saturation. A novel tangent-type PPC integrated fast fixed-time terminal sliding mode control was developed to prevent any violations of the tracking error constraint. To offset the negative effects of excessive actuator torque, an input compensator was introduced. The suggested controller is not only straightforward structurally, but also capable of guaranteeing fixed-time prescribed performance fulfillment even in the presence of input saturation. Compared with the existing fixed-time controllers, the designed control has the advantages of faster convergence rate, higher tracking precision and less control torque chattering. It is important to note that measurement noise, which deteriorates system tracking performance, is not taken into account in this research. More research needs to be undertaken with measurement noise explicitly considered in future work for tracking control of a space manipulator.

Competing interests. The authors declare that they have no Competing of known competing financial interests or personal relationships.

References

- [1] Flores Abad, A., Ma, O., Pham, K. and Ulrich, S. A review of space robotics technologies for on-orbit servicing, *Progr. Aerospace Sci.*, 2014, **68**, pp 1–26.
- [2] Rybus, T. Obstacle avoidance in space robotics: Review of major challenges and proposed solutions, *Progr. Aerospace Sci.*, 2018, **101**, pp 31–48.
- [3] Wang, H. and Xie, Y. Adaptive Jacobian position/force tracking control of free-flying manipulators, *Rob. Auton. Syst.*, 2009, **57**, (2), pp 173–181.
- [4] Nekoo, S.R. Model reference adaptive state-dependent riccati equation control of nonlinear uncertain systems: Regulation and tracking of free-floating space manipulators, *Aerospace Sci. Technol.*, 2019, **84**, pp 348–360.
- [5] Jia, Y. and Misra, A.K. Robust trajectory tracking control of a dual-arm space robot actuated by control moment gyroscopes, *Acta Astronautica*, 2017, **137**, pp 287–301.
- [6] Seddaoui, A. and Saaj, C.M. Combined nonlinear h_∞ controller for a controlled-floating space robot, *J. Guid. Control Dyn.*, 2019, **42**, (8), pp 1878–1885.
- [7] Xie, Z., Sun, T., Kwan, T. and Wu, X. Motion control of a space manipulator using fuzzy sliding mode control with reinforcement learning, *Acta Astronautica*, 2020, **176**, pp 156–172.
- [8] Jia, Q., Yuan, B., Chen, G. and Fu, Y. Adaptive fuzzy terminal sliding mode control for the free-floating space manipulator with free-swinging joint failure, *Chin. J. Aeronaut.*, 2021, **34**, (9), pp 178–198.
- [9] Kumar, N., Panwar, V. and Borm, J. Adaptive neural controller for space robot system with an attitude controlled base, *Neural Comput. Appl.*, 2013, **23**, (7-8), pp 2333–2340.
- [10] Yao, Q. Adaptive fuzzy neural network control for a space manipulator in the presence of output constraints and input nonlinearities, *Adv. Space Res.*, 2021, **67**, (6), pp 1830–1843.
- [11] Guo, Y.S. and Li, C. Terminal sliding mode control for coordinated motion of a space rigid manipulator with external disturbance, *Appl. Math. Mech.*, 2008, **029**, (5), pp 583–590.
- [12] Feng, Y., Yu, X. and Man, Z. Non-singular adaptive terminal sliding mode control of rigid manipulators, *Automatica*, 2002, **38**, pp 2159–2167.
- [13] Jia, S. and Shan, J. Finite-time trajectory tracking control of space manipulator under actuator saturation, *IEEE Trans. Ind. Electron.*, 2020, **67**, (3), pp 2086–2096.
- [14] Yang, L. and Yang, J., Nonsingular fast terminal sliding-mode control for nonlinear dynamical systems, *Int. J. Robust Nonlinear Control*, 2011, **21**, (16), pp 1865–1879.
- [15] Shao, X., Sun, G., Xue, C. and Li, X., Nonsingular terminal sliding mode control for free-floating space manipulator with disturbance, *Acta Astronautica*, 2021, **181**, pp 396–404.
- [16] Jia, S. and Shan, J. Continuous integral sliding mode control for space manipulator with actuator uncertainties, *Aerospace Sci. Technol.*, 2020, **106**, p 106192.
- [17] Polyakov, A. Nonlinear feedback design for fixed-time stabilization of linear control systems, *IEEE Trans. Autom. Control*, 2012, **57**, pp 2106–2110.
- [18] Zuo, Z. Non-singular fixed-time terminal sliding mode control of non-linear systems, *IET Control Theory Appl.*, 2015, **9**, (4), pp 545–552.

- [19] Chen, Q., Xie, S. and He, X. Neural-network-based adaptive singularity-free fixed-time attitude tracking control for spacecrafts, *IEEE Trans. Cybern.*, 2021, **51**, (10), pp 5032–5045.
- [20] Esmailzadeh, S.M., Golestani, M. and Mobayen, S. Chattering-free fault-tolerant attitude control with fast fixed-time convergence for flexible spacecraft, *Int. J. Control Autom. Syst.*, 2021, **19**, pp 767–776.
- [21] Chen, M., Wang, H. and Liu, X. Adaptive fuzzy practical fixed-time tracking control of nonlinear systems, *IEEE Trans. Fuzzy Syst.*, 2021, **29**, (3), pp 664–673.
- [22] Jin, R., Rocco, P. and Geng, Y. Observer-based fixed-time tracking control for space robots in task space, *Acta Astronautica*, 2021, **184**, pp 35–45.
- [23] Su, Y., Zheng, C. and Mercorelli, P. Robust approximate fixed-time tracking control for uncertain robot manipulators, *Mech. Syst. Signal Process.*, 2020, **135**, p 106379.
- [24] Sai, H., Xu, Z., He, S., Zhang, E. and Zhu, L. Adaptive nonsingular fixed-time sliding mode control for uncertain robotic manipulators under actuator saturation, *ISA Trans.*, 2022, **123**, pp 46–60.
- [25] He, W. and Dong, Y. Adaptive fuzzy neural network control for a constrained robot using impedance learning, *IEEE Trans. Neural Networks Learn. Syst.*, 2018, **29**, (4), pp 1174–1186.
- [26] Bechlioulis, C.P. and Rovithakis, G.A. Robust adaptive control of feedback linearizable mimo nonlinear systems with prescribed performance, *IEEE Trans. Autom. Control*, 2008, **53**, (9), pp 2090–2099.
- [27] Ilchmann, A., Ryan, E.P. and Townsend, P. Tracking control with prescribed transient behaviour for systems of known relative degree, *Syst. Control Lett.*, 2006, **55**, (5), pp 396–406.
- [28] Kostarigka, A.K., Doulgeri, Z. and Rovithakis, G.A. Prescribed performance tracking for flexible joint robots with unknown dynamics and variable elasticity, *Automatica*, 2013, **49**, (5), pp 1137–1147.
- [29] Psomopoulou, E., Theodorakopoulos, A., Doulgeri, Z. and Rovithakis, G.A. Prescribed performance tracking of a variable stiffness actuated robot, *IEEE Trans. Control Syst. Technol.*, 2015, **23**, (5), pp 1914–1926.
- [30] Bu, X., Xiao, Y. and Lei, H., An adaptive critic design-based fuzzy neural controller for hypersonic vehicles: Predefined behavioral nonaffine control, *IEEE/ASME Trans. Mechatron.*, 2019, **24**, (4), pp 1871–1881.
- [31] Bu, X., Wu, X., Huang, J. and Wei, D. Robust estimation-free prescribed performance back-stepping control of air-breathing hypersonic vehicles without affine models, *Int. J. Control*, 2016, **89**, (11), pp 2185–2200.
- [32] Bechlioulis, C.P. and Rovithakis, G.A. Decentralized robust synchronization of unknown high order nonlinear multi-agent systems with prescribed transient and steady state performance, *IEEE Trans. Autom. Control*, 2017, **62**, (1), pp 123–134.
- [33] Bu, X., Qi, Q. and Jiang, B. A simplified finite-time fuzzy neural controller with prescribed performance applied to waverider aircraft, *IEEE Trans. Fuzzy Syst.*, 2021, **30**, (7), pp 2529–2537.
- [34] Zhou, Z.G., Zhang, Y.A. and Zhou, D. Robust prescribed performance tracking control for free-floating space manipulators with kinematic and dynamic uncertainty, *Aerospace Sci. Technol.*, 2017, **71**, pp 568–579.
- [35] Zhu, Y., Qiao, J. and Guo, L. Adaptive sliding mode disturbance observer-based composite control with prescribed performance of space manipulators for target capturing, *IEEE Trans. Ind. Electron.*, 2019, **66**, pp 1973–1983.
- [36] Lu, X. and Jia, Y. Adaptive coordinated control of uncertain free-floating space manipulators with prescribed control performance, *Nonlinear Dyn.*, 2019, **97**, (2), pp 1541–1566.
- [37] Ma, H., Zhou, Q., Li, H. and Lu, R. Adaptive prescribed performance control of a flexible-joint robotic manipulator with dynamic uncertainties, *IEEE Trans. Cybern.*, 2021, **52**, (12), pp 12905–12915.
- [38] Xu, B., Ji, S., Zhang, C., Chen, C., Ni, H. and Wu, X. Linear-extended-state-observer-based prescribed performance control for trajectory tracking of a robotic manipulator, *Ind. Robot Int. J. Rob. Res. Appl.*, 2021, **48**, (4), pp 544–555.
- [39] An, S.Y., Chen, M., Wang, H.Q. and Wu, L.B. Fast finite-time dynamic surface tracking control of a single-joint manipulator system with prescribed performance, *Int. J. Syst. Sci.*, 2021, **52**, (8), pp 1551–1563.
- [40] Huang, Y. and Jia, Y. Adaptive fixed-time relative position tracking and attitude synchronization control for non-cooperative target spacecraft fly-around mission, *J. Franklin Inst.*, 2017, **354**, (18), pp 8461–8489.
- [41] Ni, J., Liu, L., Liu, C., Hu, X. and Li, S. Fast fixed-time nonsingular terminal sliding mode control and its application to chaos suppression in power system, *IEEE Trans. Circuits Syst. II Express Briefs*, 2017, **64**, (2), pp 151–155.
- [42] Zuo, Z. and Tie, L. A new class of finite-time nonlinear consensus protocols for multi-agent systems, *Int. J. Control*, 2014, **87**, (2), pp 363–370.
- [43] Wang, Z., Sun, Y. and Liang, B. Synchronization control for bilateral teleoperation system with position error constraints: A fixed-time approach, *ISA Trans.*, 2019, **93**, pp 125–136.
- [44] Spong, M., Hutchinson, S., Vidyasagar, M. and Skaar, S.B. Robot modeling and control, *IEEE Trans. Autom. Control*, 2007, **52**, pp 378–379.
- [45] Zhai, J. and Xu, G. A novel non-singular terminal sliding mode trajectory tracking control for robotic manipulators, *IEEE Trans. Circuits Syst. II Express Briefs*, 2021, **68**, (1), pp 391–395.
- [46] Ik Han, S. and Lee, J. Finite-time sliding surface constrained control for a robot manipulator with an unknown deadzone and disturbance, *ISA Trans.*, 2016, **65**, pp 307–318.
- [47] Zhang, Y., Tang, S. and Guo, J. Adaptive terminal angle constraint interception against maneuvering targets with fast fixed-time convergence, *Int. J. Robust Nonlinear Control*, 2018, **28**, (8), pp 2996–3014.